

# Isolating Sources of Disentanglement in Variational Autoencoders

Tian Qi Chen<sup>1,2</sup> Xuechen Li<sup>1,2</sup> Roger Grosse<sup>1,2</sup> David Duvenaud<sup>1,2</sup>

## Abstract

We decompose the evidence lower bound to show the existence of a term measuring the total correlation between latent variables. We use this to motivate the  $\beta$ -TCVAE (Total Correlation Variational Autoencoder) algorithm, a refinement and plug-in replacement of the  $\beta$ -VAE for learning disentangled representations, requiring no additional hyperparameters during training. We further propose a principled classifier-free measure of disentanglement called the mutual information gap (MIG). We perform extensive quantitative and qualitative experiments, in both restricted and non-restricted settings, and show a strong relation between total correlation and disentanglement, when the model is trained using our framework.

## 1. Introduction

Learning disentangled representations without supervision is a difficult open problem. Disentangled variables are generally considered to contain a combination of interpretable semantic information and the ability to independently act on the generative process. While the proper expression for disentanglement is a subject of philosophical debate, many believe a factorial representation, one with statistically independent variables, is a good starting point (Schmidhuber, 1992; Ridgeway, 2016; Achille & Soatto, 2017). Such a representation distills information into a compact form which is oftentimes semantically meaningful and useful for a variety of tasks (Ridgeway, 2016; Bengio et al., 2013). For instance, (Alemi et al., 2017a) have found such representations to be more generalizable and robust against adversarial attacks.

Many state-of-the-art methods for learning disentangled representations are based on re-weighting parts of an existing objective. For instance, Chen et al. (2016) claim that mutual information between the latent variables and observed data can encourage the latent variables into becoming more interpretable. Tangentially, Higgins et al. (2017) assert that encouraging independence between latent variables causes

<sup>1</sup>University of Toronto <sup>2</sup>Vector Institute. Correspondence to: Tian Qi (Ricky) Chen <rtqichen@cs.toronto.edu>.

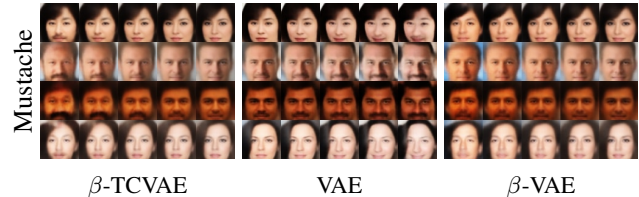


Figure 1. A  $\beta$ -TCVAE model can use a single latent variable to represent mustache while a VAE’s latent variable is entangled with smiling, but a  $\beta$ -VAE model fails to discover this attribute. A single latent variable is interpolated in each subfigure.

disentanglement. However, there is no strong evidence linking factorial representations to disentanglement. In part, this can be attributed to weaknesses of qualitative evaluation procedures. While traversals in the latent representation can illustrate disentanglement qualitatively, proper statistical measures of disentanglement can show subtle differences in models and robustness to hyperparameter settings.

Our key contributions are:

- We show a decomposition of the variational lower bound that can be used to explain the success of the  $\beta$ -VAE (Higgins et al., 2017) in learning disentangled representations.
- We propose a simple method based on weighted mini-batches to stochastically train with arbitrary weights on the terms of our decomposition without any additional hyperparameters.
- Based on this, we introduce the  $\beta$ -TCVAE, which can be used as a plug-in replacement of  $\beta$ -VAE with no extra hyperparameters. Empirical evaluations suggest that  $\beta$ -TCVAE models can discover more interpretable latent variables than existing works, while also being fairly robust to random initialization.
- We propose a new information-theoretic quantity measuring disentanglement which is classifier-free and generalizable to arbitrarily-distributed and non-scalar latent variables.

We note that Kim & Mnih (2018) have independently proposed augmenting VAEs with an equivalent total correlation penalty to the  $\beta$ -TCVAE, though their proposed training method differs from ours and requires an auxiliary discrim-

inator network. Some interesting special cases that arise from our decomposition other than  $\beta$ -TCVAE are also discussed, though we find they offer no significant performance increase in preliminary experiments (see Section 3.2.1 and ablation experiments in the Supplementary Materials).

## 2. Background

We discuss existing works that aim at either learning disentangled representations without supervision or evaluating such learned representations. The two problems are inherently related, since improvements to learning algorithms require evaluation metrics that are sensitive to subtle details, and stronger evaluation metrics reveal deficiencies in existing methods.

### 2.1. Learning Disentangled Representations

**Variational Autoencoder** The variational autoencoder (VAE) (Kingma & Welling, 2013) is a latent variable model that pairs a top-down generative model with a bottom-up inference network. Instead of directly performing maximum likelihood estimation on the intractable marginal log-likelihood, training is done by optimizing the tractable *evidence lower bound* (ELBO). We would like to optimize this lower bound averaged over the empirical distribution:

$$\mathcal{L}_{\text{ELBO}}^{\text{avg}} = \frac{1}{N} \sum_{n=1}^N (\mathbb{E}_q[\log p(x_n|z)] - \text{D}_{\text{KL}}(q(z|x_n)||p(z))). \quad (1)$$

where the decoder  $p(x_n|z)$  and encoder  $q(z|x_n)$  are parameterized by deep neural networks. For certain families of distributions, the gradients can be estimated using the *reparameterization trick*. Kingma & Welling (2013) additionally show that a properly trained VAE can disentangle emotion and pose of simple face images in the latent manifold.

**$\beta$ -VAE** The  $\beta$ -VAE (Higgins et al., 2017) is a variant of the variational autoencoder that attempts to learn a disentangled representation by optimizing a heavily penalized objective:

$$\mathcal{L}_{\beta} = \frac{1}{N} \sum_{n=1}^N (\mathbb{E}_q[\log p(x_n|z)] - \beta \text{D}_{\text{KL}}(q(z|x_n)||p(z))) \quad (2)$$

where  $\beta > 1$ . Higgins et al. (2017) argue that if  $p(z)$  is factorial then the latent representations will also be encouraged to become independent. Such simple penalization has been shown to be capable of obtaining models with a high degree of disentanglement in image datasets. However, it is not made explicit why penalizing  $\text{D}_{\text{KL}}(q(z|x)||p(z))$  with a factorial prior can lead to learning latent variables that exhibit disentangled transformations for all data samples.

**InfoGAN** The InfoGAN (Chen et al., 2016) is a variant of the generative adversarial network (GAN) (Goodfellow et al., 2014) that encourages an interpretable latent representation by maximizing the mutual information between the observation and a small subset of latent variables. The approach relies on optimizing a lower bound of the intractable mutual information.

### 2.2. Evaluating Disentangled Representations

When the true underlying generative factors are known and we have reason to believe that this set of factors is disentangled, then it is possible to create a supervised evaluation metric. Many have proposed classifier-based metrics for assessing the quality of disentanglement (Grathwohl & Wilson, 2016; Higgins et al., 2017; Kim & Mnih, 2018; Cian Eastwood, 2018; Glorot et al., 2011; Karaletsos et al., 2016). We focus on discussing the metrics proposed by Higgins et al. (2017) and Kim & Mnih (2018) as they are relatively simple in design and generalizable.

The Higgins et al. (2017) metric is defined as the accuracy that a low VC-dimension linear classifier can achieve at identifying a fixed ground truth factor. Specifically, for a set of ground truth factors  $\{v_k\}_{k=1}^K$ , each training data point is an aggregation over  $L$  samples:  $\frac{1}{L} \sum_{l=1}^L |z_l^{(1)} - z_l^{(2)}|$ , where random vectors  $z_l^{(1)}, z_l^{(2)}$  are drawn i.i.d. from  $q(z|v_k)$ <sup>1</sup> for any fixed value of  $v_k$ , and a classification target  $k$ . A drawback of this method is the lack of axis-alignment detection. That is, we believe a truly disentangled model should only contain one latent variable that is related to each factor. As a means to include axis-alignment detection, Kim & Mnih (2018) proposes using  $\text{argmin}_j \text{Var}_{q(z_j|v_k)}(z_j)$  and a majority-vote classifier.

Classifier-based disentanglement metrics tend to be ad hoc and can produce varying results depending on hyperparameters. Both the Higgins et al. (2017) and Kim & Mnih (2018) metrics can be loosely interpreted as measuring the reduction in entropy of  $z$  if  $v$  is observed. In section 4, we show that it is possible to directly measure the mutual information between  $z$  and  $v$  which is a principled information-theoretic quantity that can be used for any latent distributions provided that efficient estimation exists.

## 3. Sources of Disentanglement in the ELBO

As evidenced by Chen et al. (2016) and Higgins et al. (2017), we have reason to conjecture that the following two criteria may be of importance in learning a disentangled representation:

<sup>1</sup>Note that  $q(z|v_k)$  is sampled by using an intermediate data sample:  $z \sim q(z|x), x \sim p(x|v_k)$ .

$$\begin{aligned}
 \mathbb{E}_{p(n)} \left[ \text{D}_{\text{KL}}(q(z|n)||p(z)) \right] &= \mathbb{E}_{q(z,n)} \left[ \log q(z|n) + \log p(z) + \log q(z) - \log q(z) + \log \prod_j q(z_j) - \log \prod_j q(z_j) \right] \\
 &= \underbrace{\text{D}_{\text{KL}}(q(z,n)||q(z)p(n))}_{\text{(i) Index-Code MI}} + \underbrace{\text{D}_{\text{KL}}(q(z)||\prod_j q(z_j))}_{\text{(ii) Total Correlation}} + \underbrace{\sum_j \text{D}_{\text{KL}}(q(z_j)||p(z_j))}_{\text{(iii) Dimension-wise KL}}
 \end{aligned} \tag{3}$$

- (i) Mutual information between the latent variables and the data variable.
- (ii) Independence between the latent variables.

Hoffman & Johnson (2016) analyzed an ELBO decomposition, showcasing a term that quantifies criterion (i). In this section, we introduce a refined decomposition showing that terms describing both criteria appear in the ELBO.

### 3.1. ELBO TC-Decomposition

Following the notation in the decomposition by Hoffman & Johnson (2016), we identify each training example with a unique integer index and define a uniform random variable on  $\{1, 2, \dots, N\}$  with which we relate to data points. Furthermore, we define  $q(z|n) = q(z|x_n)$  and  $q(z, n) = q(z|n)p(n) = q(z|n)\frac{1}{N}$ . We refer to  $q(z) = \sum_{n=1}^N q(z|n)p(n)$  as the *aggregated posterior* following Makhzani et al. (2016), which captures the aggregate structure of the latent variables under the data distribution. With such notation, we decompose the KL term in (1) assuming a factorized  $p(z)$ . The decomposition is shown in (3) where  $z_j$  denotes the  $j$ th dimension of the latent variable (see Supplementary Materials for derivation). Immediately we see that the effect of the prior is only a dimension-wise regularization, and there exist terms that enforce the aggregate posterior  $q(z)$  to satisfy certain statistical properties.

#### 3.1.1. DECOMPOSITION ANALYSIS

In a similar decomposition, Hoffman & Johnson (2016) refer to (i) as the *index-code mutual information* (MI). The index-code MI is the mutual information  $I_q(z; n)$  between the data variable and latent variable based on the empirical data distribution  $q(z, n)$ . In fact, (i) can be viewed as a consistent but biased estimator for the mutual information between  $p(x)$  and  $q(z)$  under the true data generating distribution, as the expectation of the index-code MI is a lower bound. Since  $p(n)$  here is the empirical data distribution, the subtlety is that a higher index-code MI would imply the latent variables have sufficient information for distinguishing the empirical samples. Chen et al. (2016) have argued that a higher mutual information can lead to disentanglement, and some have even proposed completely disregarding this

term (Makhzani et al., 2016; Zhao et al., 2017).

In information theory, (ii) is referred to as the *total correlation* (TC), one of many generalizations of mutual information to more than two random variables (Watanabe, 1960). The naming is unfortunate as it is actually a measure of dependence between the variables. The penalty on TC forces the model to find statistically independent factors in the data distribution. We argue that a heavier penalty on this term causes each dimension of the aggregate posterior to learn statistically independent semantics in the data distribution, which induces a more disentangled representation.

We refer to (iii) as the *dimension-wise KL*. This term mainly prevents the individual latent dimensions from deviating too far from their corresponding priors. It acts as a complexity penalty on the aggregate posterior which reasonably follows from the minimum description length (Hinton & Zemel, 1994) formulation of the ELBO.

A special case of this decomposition was proven by Achille & Soatto (2018) after assuming that the use of a flexible prior can effectively ignore the dimension-wise KL term. In contrast, our decomposition (3) is more generally applicable to many applications of the evidence lower bound.

#### 3.1.2. ANALYZING THE $\beta$ -VAE

Recall that the  $\beta$ -VAE increases the penalty on the average-of-KL's term in the vanilla ELBO. In the context of our decomposition, this corresponds to increasing the weight on all three terms. More specifically, this means the objective encourages low total correlation but simultaneously penalizes the index-code mutual information.

We hypothesize that a low total correlation is the main reason  $\beta$ -VAE achieves empirical success in learning disentangled representations. However, more importantly, we should emphasize that because  $\beta$ -VAE penalizes the index-code mutual information by the same weight, it cannot obtain low total correlation without also obtaining a low index-code MI. This encourages the model to discard information from the latent variables, resulting in poor use of the latent variables in the generative model. Such reasoning resonates with the observed behavior that  $\beta$  is a hyperparameter that requires careful tuning and that large  $\beta$  values typically fail

in practice (Higgins et al., 2017; Alemi et al., 2017b).

From this reasoning, it may be advantageous to amplify the penalization on only the total correlation term as the other terms are counterproductive or irrelevant to learning disentangled representations. We note that Kim & Mnih (2018) have independently proposed a learning algorithm that penalizes the total correlation of latent variables without additional penalty on the index-code MI, which is a special case of this decomposition. During training, they require an inner optimization loop for an auxiliary discriminator network used in the density ratio trick (Sugiyama et al., 2012). In the following section, we propose a simple yet general method for training with the TC-decomposition using minibatches of data.

### 3.2. Training with Minibatch Weighted Sampling

We describe a method to stochastically estimate the decomposition terms, which will allow scalable training with arbitrary weights for each decomposition term. Note that the decomposed expression (3) requires the evaluation of the density function  $q(z) = \mathbb{E}_{p(n)}[q(z|n)]$ , which depends on the entire empirical dataset<sup>2</sup>. As such, it is undesirable to compute it exactly during training. One main advantage of our stochastic estimation method is the lack of hyperparameters or inner optimization loops, which should provide more stable training.

First notice that a naïve Monte Carlo approximation based on a minibatch of samples from  $p(n)$  is very likely to underestimate  $q(z)$ . This can be intuitively seen by viewing  $q(z)$  as a mixture distribution where the data index  $n$  indicates the mixture component. With a randomly sampled component,  $q(z|n)$  is close to 0, whereas  $q(z|n)$  would be large if  $n$  is the component that  $z$  came from. So it is much better to sample this component and weight the probability appropriately.

To this end, we propose using a weighted version for estimating the function  $\log q(z)$  during training, inspired by importance sampling. When provided with a minibatch of samples  $\{n_1, \dots, n_M\}$ , we can use the estimator

$$\mathbb{E}_{q(z)}[\log q(z)] \approx \frac{1}{M} \sum_{i=1}^M \left[ \log \frac{1}{NM} \sum_{j=1}^M q(z(n_i)|n_j) \right] \quad (4)$$

where  $z(n_i)$  is a sample from  $q(z|n_i)$  (see derivation in Supplementary Materials).

Note that while this minibatch estimator is biased since its

<sup>2</sup>The same argument holds for the term  $\prod_j q(z_j)$  and a similar estimator can be constructed.

expectation is a lower bound<sup>3</sup>. Despite this bias, we note that this simple trick is crucial for enabling training, and it can be advantageous due to the absence of any additional hyperparameters.

#### 3.2.1. $\beta$ -TCVAE

With minibatch weighted sampling, it is possible to assign different penalty weights to the terms in (3).

$$\begin{aligned} \mathcal{L}_{\beta\text{-TC}} := & \frac{1}{N} \sum_{n=1}^N (\mathbb{E}_{q(z|n)}[\log p(n|z)]) - \alpha I_q(z; n) \\ & - \beta \mathbf{D}_{\text{KL}}(q(z) \| \prod_j q(z_j)) \\ & - \gamma \sum_j \mathbf{D}_{\text{KL}}(q(z_j) \| p(z_j)) \end{aligned} \quad (5)$$

We combine the preceding insights regarding our decomposition into the  $\beta$ -TCVAE model by using  $\alpha = \gamma = 1$  and only tuning  $\beta$  (see some ablation studies regarding  $\alpha$  and  $\gamma$  in the Supplementary Materials).

## 4. Measuring Disentanglement with MIG

It is difficult to compare disentangling algorithms without a proper metric. Most prior works have resorted to visualizing the effects of change in the representation. This is tedious and cannot be used to measure the robustness of an approach. Furthermore, a metric should itself be robust to hyperparameters so that properties of robustness (or lack thereof) can be properly attributed to the algorithm. Existing classifier-based metrics use simple classifier to reduce the amount of variance, but the necessity of designing a dataset is not hyperparameter-free and can bias the metric value (see Supplementary Materials).

We can measure a notion of disentanglement when the empirical generative process  $p(n|v)$  and its ground truth latent factors  $v$  are known. Often these are semantically meaningful scalar attributes of the data sample. For instance, photographic portraits generally contain disentangled factors such as pose (azimuth and elevation), lighting condition, and attributes of the face such as skin tone, gender, face width, etc. Though not all ground truth factors may be provided, it is still possible to evaluate disentanglement using the known factors. To this end, we propose a metric based on the empirical mutual information between latent variables and ground truth factors.

### 4.1. Mutual Information Gap (MIG)

Our key insight is that the *empirical mutual information* between a latent variable  $z_j$  and a ground truth factor  $v_k$

<sup>3</sup>This follows from Jensen’s inequality  $\mathbb{E}_{p(n)}[\log q(z|n)] \leq \log \mathbb{E}_{p(n)}[q(z|n)]$ .

Disentanglement Metric	Axis	Unbiased	General
Higgins et al. (2017)	No	No	No
Kim & Mnih (2018)	Yes	No	No
MIG (Ours)	Yes	Yes	Yes

Table 1. In comparison to prior metrics, our proposed MIG detects axis-alignment, is unbiased for all hyperparameter settings, and can be generally applied to any latent distributions provided efficient estimation exists.

can be estimated using the joint distribution defined by  $q(z_j, v_k) = \sum_{n=1}^N p(v_k)p(n|v_k)q(z_j|n)$ . Assuming that the underlying factors  $p(v_k)$  and the generating process is known for the empirical data samples  $p(n|v_k)$ , then

$$I_n(z_j; v_k) = \mathbb{E}_{q(z_j, v_k)} \left[ \log \sum_{n \in \mathcal{X}_{v_k}} q(z_j|n)p(n|v_k) \right] + H(z_j) \quad (6)$$

where  $\mathcal{X}_{v_k}$  is the support of  $p(n|v_k)$ . (See derivation in Supplementary Materials.)

The mutual information is an information-theoretic quantity able to describe the relationship between  $z_j$  and  $v_k$  regardless of their parameterization. A higher mutual information implies that  $z_j$  contains a lot of information about  $v_k$ , and the mutual information is maximal if there exists an invertible relationship between  $z_j$  and  $v_j$ . Furthermore, for quantized  $v_k$ , the mutual information is bounded  $0 \leq I(z_j; v_k) \leq H(v_k)$ , where  $H(v_k) = \mathbb{E}_{p(v_k)}[-\log p(v_k)]$  is the entropy of  $v_k$ . As such, we use the normalized mutual information  $I(z_j; v_k)/H(v_k)$ .

Note that a single factor can have high mutual information with multiple latent variables. We enforce an axis-alignment detection by measuring the difference between the top two latent variables with highest mutual information. The full metric we call *mutual information gap* (MIG) is then

$$\frac{1}{K} \sum_{k=1}^K \frac{1}{H(v_k)} \left( I_n(z_{j^{(k)}}; v_k) - \max_{j \neq j^{(k)}} I_n(z_j; v_k) \right) \quad (7)$$

where  $j^{(k)} = \operatorname{argmax}_j I_n(z_j; v_k)$  and  $K$  is the number of known factors. MIG is bounded between 0 and 1.

While it is possible to compute just the average maximal MI,  $\frac{1}{K} \sum_{k=1}^K \frac{I_n(z_{k^*}; v_k)}{H(v_k)}$ , the gap in our formulation (7) defends against two important cases. The first case is related to rotation of the factors. When a set of latent variables are not axis-aligned, each variable can contain a decent amount of information regarding two or more factors. The gap heavily penalizes unaligned variables, which is an indication of entanglement. The second case is related to compactness of

the representation. If one latent variable reliably models a ground truth factor, then it is unnecessary for other latent variables to also be informative about this factor.

As summarized in Table 1, our metric detects axis-alignment and is generally applicable and meaningful for any factorized latent distribution, including vectors of multimodal, Categorical, and other structured distributions. This is because the metric is only limited by whether the mutual information can be estimated. Efficient estimation of mutual information is an ongoing research topic (Belghazi et al., 2018; Reshef et al., 2011), but we find that the simple estimator (6) is sufficient for the datasets we use. We find that MIG can better capture subtle differences in models compared to existing metrics. Systematic experiments analyzing MIG and existing metrics are placed in the Supplementary Materials.

## 5. Related Work

We focus on discussing the learning of disentangled representations in an unsupervised manner. Nevertheless, we note that inverting generative processes with known disentangled factors through weak supervision has been pursued by many. The goal in this case is not perfect inversion but to distill into a simpler representation (Hinton et al., 2011; Kulkarni et al., 2015; Cheung et al., 2014; Karaletsos et al., 2016; Vedantam et al., 2018). Although not explicitly the main motivation, many unsupervised generative modeling frameworks have explored the disentanglement of their learned representations (Kingma & Welling, 2013; Makhzani et al., 2016; Radford et al., 2015). Prior to  $\beta$ -VAE (Higgins et al., 2017), some have shown successful disentanglement in limited settings with few factors of variation (Schmidhuber, 1992; Tang et al., 2013; Desjardins et al., 2012; Glorot et al., 2011).

With recent progress in generative modeling, Chen et al. (2016) propose the InfoGAN by modifying the generative adversarial networks objective (Goodfellow et al., 2014) to encourage high mutual information between a small subset of latent variables and the observed data. This motivates the removal of the index-code MI term in (3) which is explored in some recent works (Makhzani et al., 2016; Zhao et al., 2017). However, investigations into generative modeling also claim that a penalized mutual information through the information bottleneck encourages compact and disentangled representations (Achille & Soatto, 2017; Burgess et al., 2017).

As a means to describe the properties of disentangled representations, factorial representations have been motivated by many (Schmidhuber, 1992; Ridgeway, 2016; Achille & Soatto, 2017, 2018; Ver Steeg & Galstyan, 2015; Kumar et al., 2017). In particular, Appendix B of Achille &

Dataset	Ground truth factors
dSprites	scale (6), rotation (40), posX (32), posY (32)
3D Faces	azimuth (21), elevation (11), lighting (11)

Table 2. Summary of datasets with known ground truth factors. Parentheses contain number of quantized values for each factor.

Soatto (2018) show the existence of total correlation in a similar objective with a flexible prior and assuming optimality  $q(z) = p(z)$ . Similarly, Gao et al. (2018) arrives at the ELBO from an objective that simultaneously maximizes informativeness and minimizes the total correlation of latent variables. In contrast, we show a more general analysis of the unmodified evidence lower bound.

As previously mentioned, the existence of the index-code MI in the ELBO is known (Hoffman & Johnson, 2016), and as a result Kim & Mnih (2018) have independently proposed FactorVAE, which uses an equivalent objective to the  $\beta$ -TCVAE. The main difference is they estimate total correlation using the density ratio trick (Sugiyama et al., 2012) which requires an auxiliary discriminator network and an inner optimization loop. In contrast, we emphasize the success of  $\beta$ -VAE using our refined decomposition, and we propose a training method that allows assigning arbitrary weights to each term of the objective without requiring any additional networks. We show in our experiments that the  $\beta$ -TCVAE is more stable and can achieve better disentangled representations on some datasets.

In a similar vein, non-linear independent component analysis (Comon, 1994; Hyvärinen & Pajunen, 1999; Jutten & Karhunen, 2003) studies the problem of inverting a generative process assuming independent latent factors. Instead of a perfect inversion, we only aim for maximizing the mutual information between our learned representation and the ground truth factors. Simple priors can further encourage interpretability by means of warping complex factors into simpler manifolds. To the best of our knowledge, we are the first to show a strong quantifiable relation between factorial representations and disentanglement (see Section 6.1.3).

## 6. Experiments

We perform a series of quantitative and qualitative experiments, showing that  $\beta$ -TCVAE can consistently achieve higher MIG scores compared to two of the state-of-the-art methods,  $\beta$ -VAE (Higgins et al., 2017) and InfoGAN (Chen et al., 2016). Furthermore, we find that in models trained with our method, total correlation is strongly correlated with disentanglement. Our experimental settings follow closely from Higgins et al. (2017); see Supplementary Materials for exact details.

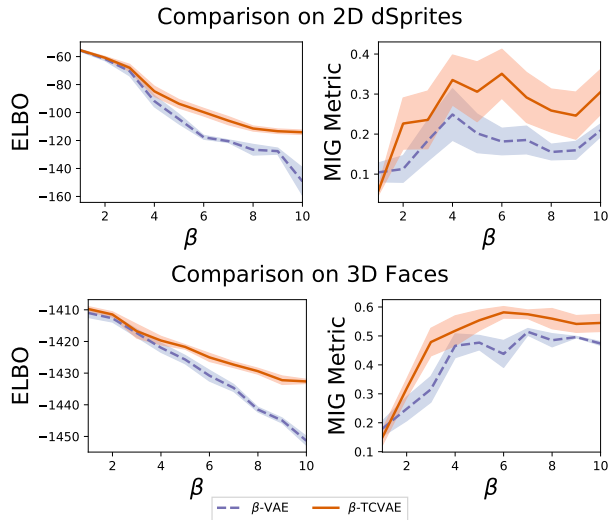


Figure 2. Compared to  $\beta$ -VAE,  $\beta$ -TCVAE creates more disentangled representations while preserving a better generative model of the data with increasing  $\beta$ . Shaded regions show the 90% confidence intervals. Higher is better on both metrics.

### 6.1. Independent Factors of Variation

First, we analyze the performance of our proposed  $\beta$ -TCVAE and MIG metric in a restricted setting, with ground truth factors that are uniformly and independently sampled. To paint a clearer picture on the robustness of learning algorithms, we aggregate results from multiple experiments to visualize the effect of initialization.

We perform quantitative evaluations with two datasets, a dataset of 2D shapes (Matthey et al., 2017) and a dataset of synthetic 3D faces (Paysan et al., 2009). Their ground truth factors are summarized in Table 2. The dSprites and 3D faces also contain 3 types of shapes and 50 identities, respectively, which are treated as noise during evaluation.

#### 6.1.1. ELBO VS. DISENTANGLEMENT TRADE-OFF

Since the  $\beta$ -VAE and  $\beta$ -TCVAE objectives are lower bounds on the standard ELBO, we would like to see the effect of training with this modification. To see how the choice of  $\beta$  affects these learning algorithms, we train using a range of values. The trade-off between density estimation and the amount of disentanglement measured by MIG is shown in Figure 2.

We find that  $\beta$ -TCVAE provides a better trade-off between density estimation and disentanglement. Notably, with higher values of  $\beta$ , the mutual information penalty in  $\beta$ -VAE is too strong and this hinders the usefulness of the latent variables. However,  $\beta$ -TCVAE with higher values of  $\beta$  consistently results in models with higher disentanglement score relative to  $\beta$ -VAE.

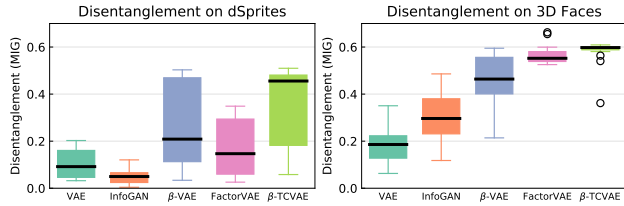


Figure 3. Distribution of disentanglement score (MIG) for different modeling algorithms.

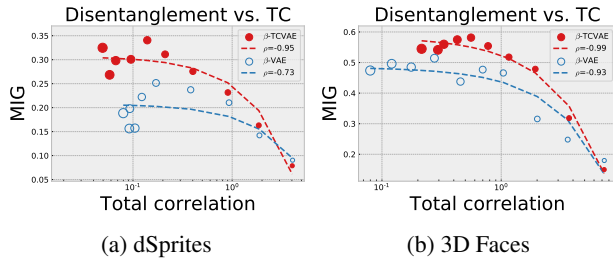
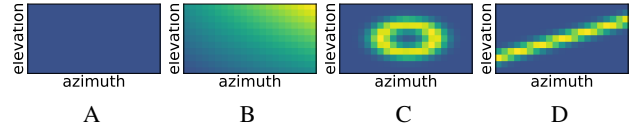


Figure 4. Scatter plots of the average MIG and TC per value of  $\beta$ . Larger circles indicate a higher  $\beta$ . On average,  $\beta$ -TCVAE makes better use of low total correlation scores to reach higher disentanglement. Note the log-scale for TC, though the Pearson correlation coefficients  $\rho$  are estimated without using log.

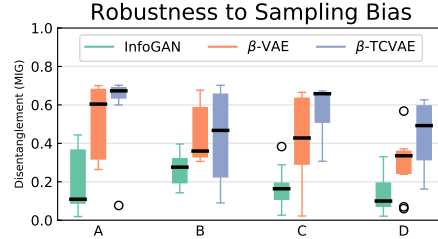
### 6.1.2. QUANTITATIVE COMPARISONS

While a disentangled representation may be achievable by some learning algorithms, the chances of obtaining such a representation typically is not clear. Unsupervised learning of a disentangled representation can have high variance since disentangled labels are not provided during training. To further understand the robustness of each algorithm, we show box plots depicting the quartiles of the MIG score distribution for various methods in Figure 3. We used  $\beta = 4$  for  $\beta$ -VAE and  $\beta = 6$  for  $\beta$ -TCVAE, based on modes in Figure 2. For InfoGAN, we used 5 continuous latent codes and 5 noise variables. Other settings are chosen following those suggested by Chen et al. (2016), but we also added instance noise (Sønderby et al., 2017) to stabilize training. FactorVAE uses an equivalent objective to the  $\beta$ -TCVAE but is trained with the density ratio trick (Sugiyama et al., 2012), which is known to underestimate the TC term (Kim & Mnih, 2018). As a result, we tuned  $\beta \in [1, 80]$  and used double the number of iterations for FactorVAE. Note that while  $\beta$ -VAE, FactorVAE and  $\beta$ -TCVAE use a fully connected architecture for the dSprites dataset, InfoGAN uses a convolutional architecture for increased stability; specifics are described in the Supplementary Materials.

Despite our best efforts, we were unable to train InfoGAN to disentangle the dSprites dataset even when using the more stable convolutional architecture. This is likely due to pixels of input images only take on binary values in



(a) Different joint distributions of factors.



(b) Distribution of disentanglement scores (MIG).

Figure 5. The  $\beta$ -TCVAE has a higher chance of obtaining a disentangled representation than  $\beta$ -VAE, even in the presence of sampling bias. (a) All samples have non-zero probability in all joint distributions; the most likely sample is 4 times as likely as the least likely sample.

$\{0, 1\}$ , which required the instance noise trick to even begin training. We also find that FactorVAE performs poorly with fully connected layers, resulting in worse results than  $\beta$ -VAE on the dSprites dataset.

In general, we find that the median score is highest for  $\beta$ -TCVAE and it is close to the highest score achieved by all methods. Despite the best half of the  $\beta$ -TCVAE runs achieving relatively high scores, we see that the other half can still perform poorly. Low-score outliers exist in the 3D faces dataset, although their scores are still higher than the median scores achieved by both VAE and InfoGAN.

### 6.1.3. FACTORIAL VS. DISENTANGLED REPRESENTATIONS

While a low total correlation has been previously conjectured to lead to disentanglement, we provide concrete evidence that our  $\beta$ -TCVAE learning algorithm satisfies this property. Figure 4 shows a scatter plot of total correlation and the MIG disentanglement metric for varying values of  $\beta$  trained on the dSprites and faces datasets, averaged over 40 random initializations. For models trained with  $\beta$ -TCVAE, the correlation between average TC and average MIG is strongly negative, while models trained with  $\beta$ -VAE have a weaker correlation. For the dSprites data, we see that with higher values of  $\beta$ ,  $\beta$ -VAE seems to stop decreasing the TC among latent variables while disentanglement further decreases. Meanwhile,  $\beta$ -VAE achieves a lower total correlation than  $\beta$ -TCVAE on the 3D faces dataset, possibly an indication of latent variables regressing towards the prior and becoming inactive. In general, for the same degree of

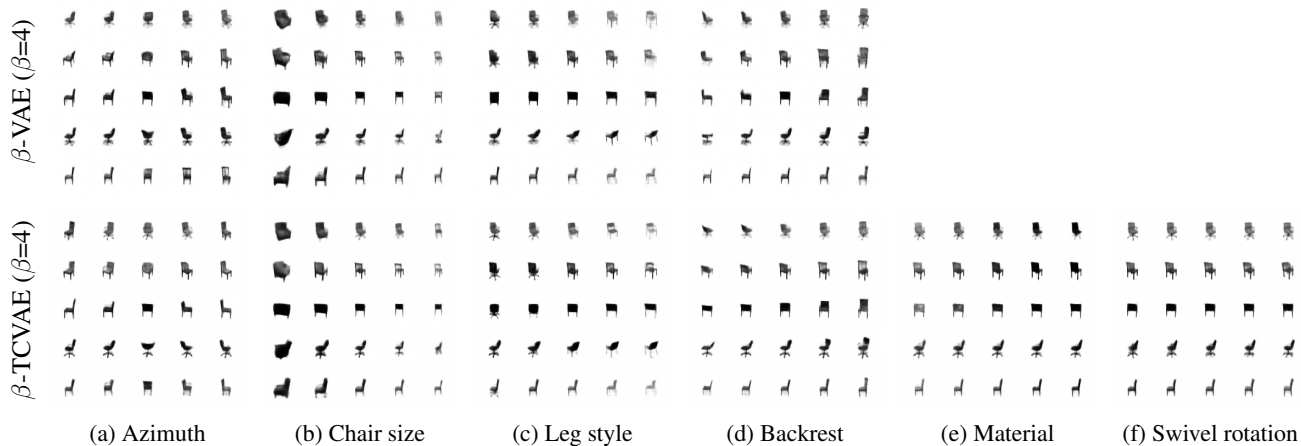


Figure 6. Learned latent variables using  $\beta$ -VAE and  $\beta$ -TCVAE are shown. Traversal range is  $(-2, 2)$ .

total correlation,  $\beta$ -TCVAE creates a better disentangled model. This is also strong evidence for the hypothesis that large values of  $\beta$  can be useful as long as the index-code mutual information is not penalized.

## 6.2. Correlated or Dependent Factors

A notion of disentanglement can exist even when the underlying generative process samples factors non-uniformly and dependently sampled. Many real datasets exhibit this behavior, where some configurations of factors are sampled more than others, violating the statistical independence assumption. Disentangling the factors of variation in this case corresponds to finding the generative model where the latent factors can independently act and perturb the generated result, even when there is bias in the sampling procedure. In general, we find that  $\beta$ -TCVAE has no problem in finding the correct factors of variation in a toy dataset and can find more interpretable factors of variation than those found in prior work, even though the independence assumption is violated.

### 6.2.1. 2D FACTORS

We start off with a toy dataset with only two factors and test  $\beta$ -TCVAE using sampling distributions with varying degrees of correlation and dependence. We take the dataset of synthetic 3D faces and fix the lighting factor. The joint distributions over factors that we test with are summarized in Figure 5a, which includes varying degrees of sampling bias. Specifically, configuration A uses uniform and independent factors; B uses factors with non-uniform marginals but are uncorrelated and independent; C uses uncorrelated but dependent factors; and D uses correlated and dependent factors.

For each method, we train 10 models and compute their

MIG. Due to the reduction from three to two factors, we find that  $\beta = 4$  is enough to give reasonable results for both  $\beta$ -VAE and  $\beta$ -TCVAE. For InfoGAN, we used 2 continuous codes and 8 noise variables. Box plots showing the quartiles for each configuration are shown in Figure 5. While it is possible to train a disentangled model in all configurations, the chances of obtaining one is overall lower when there exist sampling bias. Across all configurations, we see that  $\beta$ -TCVAE is superior to  $\beta$ -VAE and InfoGAN, and there is a large difference in median scores for most configurations.

### 6.2.2. QUALITATIVE COMPARISONS

We find that  $\beta$ -TCVAE can discover more disentangled factors than  $\beta$ -VAE on datasets of chairs (Aubry et al., 2014) and real faces (Liu et al., 2015). We qualitatively compare traversals in the latent space.

**3D Chairs** Figure 6 shows traversals in latent variables that depict an interpretable property in generating 3D chairs. The  $\beta$ -VAE (Higgins et al., 2017) has shown to be capable of learning the first four properties: azimuth, size, leg style, and backrest. However, the leg style change learned by  $\beta$ -VAE does not seem to be consistent for all chairs. We find that  $\beta$ -TCVAE can learn two additional interpretable properties: material of the chair, and leg rotation for swivel chairs. These two properties are more subtle and likely require a higher index-code mutual information, so the lower penalization of index-code MI in  $\beta$ -TCVAE helps in finding these properties.

**CelebA** Figure 7 shows 4 out of more than 10 attributes that are discovered by the  $\beta$ -TCVAE without supervision (see more in Supplementary Materials). We traverse in a large range to show the effect of generalizing the represented semantics of each variable. The representation learned by  $\beta$ -VAE is entangled with nuances, which can be





Figure 7. Qualitative comparisons on CelebA. Traversal ranges are shown in parentheses. Some attributes are only manifested in one direction of a latent variable, so we show a one-sided traversal. Most semantically similar variables from a  $\beta$ -VAE are shown for comparison.

shown when generalizing to low probability regions. For instance, it has difficulty rendering complete baldness or narrow face width, whereas the  $\beta$ -TCVAE shows meaningful extrapolation. The extrapolation of the gender attribute of  $\beta$ -TCVAE shows that it focuses more on gender-specific facial features, whereas the  $\beta$ -VAE is entangled with many irrelevances such as face width. The ability to generalize beyond the first few standard deviations of the prior mean implies that the  $\beta$ -TCVAE model can generate rare samples such as *bald or mustached females*.

## 7. Conclusion

We present a decomposition of the ELBO with the goal of explaining why  $\beta$ -VAE works. In particular, we find that a TC penalty in the objective encourages the model to find statistically independent factors in the data distribution. We then designate a special case as  $\beta$ -TCVAE, which can be trained stochastically using minibatch estimator with no additional hyperparameters compared to the  $\beta$ -VAE. To quantitatively evaluate our approach, we propose a classifier-free disentanglement metric called MIG. We show that  $\beta$ -TCVAE is superior to  $\beta$ -VAE and InfoGAN in learning disentangled representations, and can more robustly disentangle than FactorVAE. Unsupervised learning of disentangled representations is inherently a difficult problem due to the lack of a prior for semantic awareness, but we show some evidence in simple datasets with uniform factors that independence between latent variables can be strongly related to disentanglement.

## Acknowledgements

We thank Alireza Makhzani, Yuxing Zhang, and Bowen Xu for initial discussions. We also thank Chatavut Viriyasuthee for pointing out an error in one of our derivations. TQC would also like to thank Brendan Shillingford for supplying complementary accommodation at a popular conference.

## References

- Achille, Alessandro and Soatto, Stefano. On the emergence of invariance and disentangling in deep representations. *arXiv preprint arXiv:1706.01350*, 2017.
- Achille, Alessandro and Soatto, Stefano. Information dropout: Learning optimal representations through noisy computation. *IEEE Transactions on Pattern Analysis and Machine Intelligence*, 2018.
- Alemi, Alexander A, Fischer, Ian, Dillon, Joshua V, and Murphy, Kevin. Deep variational information bottleneck. *International Conference on Learning Representations*, 2017a.
- Alemi, Alexander A, Poole, Ben, Fischer, Ian, Dillon, Joshua V, Saurous, Rif A, and Murphy, Kevin. An information-theoretic analysis of deep latent-variable models. *arXiv preprint arXiv:1711.00464*, 2017b.
- Aubry, Mathieu, Maturana, Daniel, Efros, Alexei, Russell, Bryan, and Sivic, Josef. Seeing 3d chairs: exemplar part-based 2d-3d alignment using a large dataset of cad models. In *CVPR*, 2014.
- Belghazi, Ishmael, Rajeswar, Sai, Baratin, Aristide, Hjelm, R Devon, and Courville, Aaron. MINE: Mutual informa-

- tion neural estimation. *arXiv preprint arXiv:1801.04062*, 2018.
- Bengio, Yoshua, Courville, Aaron, and Vincent, Pascal. Representation learning: A review and new perspectives. *IEEE transactions on pattern analysis and machine intelligence*, 35(8):1798–1828, 2013.
- Burda, Yuri, Grosse, Roger, and Salakhutdinov, Ruslan. Importance weighted autoencoders. *arXiv preprint arXiv:1509.00519*, 2015.
- Burgess, Christopher, Higgins, Irina, Pal, Arka, Matthey, Loic, Watters, Nick, Desjardins, Guillaume, and Lerchner, Alexander. Understanding disentangling in beta-vae. *Learning Disentangled Representations: From Perception to Control Workshop*, 2017.
- Chen, Xi, Duan, Yan, Houthoofd, Rein, Schulman, John, Sutskever, Ilya, and Abbeel, Pieter. Infogan: Interpretable representation learning by information maximizing generative adversarial nets. In *Advances in Neural Information Processing Systems*, pp. 2172–2180, 2016.
- Cheung, Brian, Livezey, Jesse A, Bansal, Arjun K, and Olshausen, Bruno A. Discovering hidden factors of variation in deep networks. *arXiv preprint arXiv:1412.6583*, 2014.
- Cian Eastwood, Christopher K. I. Williams. A framework for the quantitative evaluation of disentangled representations. *International Conference on Learning Representations*, 2018.
- Comon, Pierre. Independent component analysis, a new concept? *Signal processing*, 36(3):287–314, 1994.
- Desjardins, Guillaume, Courville, Aaron, and Bengio, Yoshua. Disentangling factors of variation via generative entangling. *arXiv preprint arXiv:1210.5474*, 2012.
- Gao, Shuyang, Brekelmans, Rob, Ver Steeg, Greg, and Galstyan, Aram. Auto-encoding total correlation explanation. *arXiv preprint arXiv:1802.05822*, 2018.
- Glorot, Xavier, Bordes, Antoine, and Bengio, Yoshua. Domain adaptation for large-scale sentiment classification: A deep learning approach. In *Proceedings of the 28th international conference on machine learning (ICML-11)*, pp. 513–520, 2011.
- Goodfellow, Ian, Pouget-Abadie, Jean, Mirza, Mehdi, Xu, Bing, Warde-Farley, David, Ozair, Sherjil, Courville, Aaron, and Bengio, Yoshua. Generative adversarial nets. In *Advances in neural information processing systems*, pp. 2672–2680, 2014.
- Goroshin, Ross, Mathieu, Michael F, and LeCun, Yann. Learning to linearize under uncertainty. In *Advances in Neural Information Processing Systems*, pp. 1234–1242, 2015.
- Grathwohl, Will and Wilson, Aaron. Disentangling space and time in video with hierarchical variational autoencoders. *arXiv preprint arXiv:1612.04440*, 2016.
- Higgins, Irina, Matthey, Loic, Pal, Arka, Burgess, Christopher, Glorot, Xavier, Botvinick, Matthew, Mohamed, Shakir, and Lerchner, Alexander. beta-vae: Learning basic visual concepts with a constrained variational framework. *International Conference on Learning Representations*, 2017.
- Hinton, Geoffrey E and Zemel, Richard S. Autoencoders, minimum description length and helmholtz free energy. In *Advances in neural information processing systems*, pp. 3–10, 1994.
- Hinton, Geoffrey E, Krizhevsky, Alex, and Wang, Sida D. Transforming auto-encoders. In *International Conference on Artificial Neural Networks*, pp. 44–51. Springer, 2011.
- Hoffman, Matthew D and Johnson, Matthew J. Elbo surgery: yet another way to carve up the variational evidence lower bound. In *Workshop in Advances in Approximate Bayesian Inference, NIPS*, 2016.
- Hyvärinen, Aapo and Pajunen, Petteri. Nonlinear independent component analysis: Existence and uniqueness results. *Neural Networks*, 12(3):429–439, 1999.
- Jutten, Christian and Karhunen, Juha. Advances in nonlinear blind source separation. 2003.
- Karaletsos, Theofanis, Belongie, Serge, and Rätsch, Gunnar. Bayesian representation learning with oracle constraints. *International Conference on Learning Representations*, 2016.
- Kim, Hyunjik and Mnih, Andriy. Disentangling by factorising. *arXiv preprint arXiv:1802.05983*, 2018.
- Kingma, Diederik P and Ba, Jimmy. Adam: A method for stochastic optimization. *International Conference on Learning Representations*, 2015.
- Kingma, Diederik P and Welling, Max. Auto-encoding variational bayes. *arXiv preprint arXiv:1312.6114*, 2013.
- Kulkarni, Tejas D, Whitney, William F, Kohli, Pushmeet, and Tenenbaum, Josh. Deep convolutional inverse graphics network. In *Advances in Neural Information Processing Systems*, pp. 2539–2547, 2015.

- Kumar, Abhishek, Sattigeri, Prasanna, and Balakrishnan, Avinash. Variational inference of disentangled latent concepts from unlabeled observations. *arXiv preprint arXiv:1711.00848*, 2017.
- Liu, Ziwei, Luo, Ping, Wang, Xiaogang, and Tang, Xiaoou. Deep learning face attributes in the wild. In *Proceedings of the IEEE International Conference on Computer Vision*, pp. 3730–3738, 2015.
- Louizos, Christos, Swersky, Kevin, Li, Yujia, Welling, Max, and Zemel, Richard. The variational fair autoencoder. *arXiv preprint arXiv:1511.00830*, 2015.
- Makhzani, Alireza, Shlens, Jonathon, Jaitly, Navdeep, Goodfellow, Ian, and Frey, Brendan. Adversarial autoencoders. *ICLR 2016 Workshop, International Conference on Learning Representations*, 2016.
- Matthey, Loic, Higgins, Irina, Hassabis, Demis, and Lerchner, Alexander. dsprites: Disentanglement testing sprites dataset. <https://github.com/deepmind/dsprites-dataset/>, 2017.
- Paysan, Pascal, Knothe, Reinhard, Amberg, Brian, Romdhani, Sami, and Vetter, Thomas. A 3d face model for pose and illumination invariant face recognition. In *Advanced Video and Signal Based Surveillance, 2009. AVSS'09. Sixth IEEE International Conference on*, pp. 296–301. IEEE, 2009.
- Radford, Alec, Metz, Luke, and Chintala, Soumith. Un-supervised representation learning with deep convolutional generative adversarial networks. *arXiv preprint arXiv:1511.06434*, 2015.
- Reed, Scott, Sohn, Kihyuk, Zhang, Yuting, and Lee, Honglak. Learning to disentangle factors of variation with manifold interaction. In *International Conference on Machine Learning*, pp. 1431–1439, 2014.
- Reshef, David N, Reshef, Yakir A, Finucane, Hilary K, Grossman, Sharon R, McVean, Gilean, Turnbaugh, Peter J, Lander, Eric S, Mitzenmacher, Michael, and Sabeti, Pardis C. Detecting novel associations in large data sets. *science*, 334(6062):1518–1524, 2011.
- Ridgeway, Karl. A survey of inductive biases for factorial representation-learning. *arXiv preprint arXiv:1612.05299*, 2016.
- Schmidhuber, Jürgen. Learning factorial codes by predictability minimization. *Neural Computation*, 4(6):863–879, 1992.
- Siddharth, N, Paige, Brooks, Van de Meent, Jan-Willem, Desmaison, Alban, and Torr, Philip HS. Learning disentangled representations with semi-supervised deep generative models. *Advances in Neural Information Processing Systems*, 2017.
- Sønderby, Casper Kaae, Caballero, Jose, Theis, Lucas, Shi, Wenzhe, and Huszár, Ferenc. Amortised map inference for image super-resolution. *International Conference on Learning Representations*, 2017.
- Sugiyama, Masashi, Suzuki, Taiji, and Kanamori, Takafumi. *Density ratio estimation in machine learning*. Cambridge University Press, 2012.
- Tang, Yichuan, Salakhutdinov, Ruslan, and Hinton, Geoffrey. Tensor analyzers. In *International Conference on Machine Learning*, pp. 163–171, 2013.
- Thomas, Valentin, Pondard, Jules, Bengio, Emmanuel, Sarfati, Marc, Beaudoin, Philippe, Meurs, Marie-Jean, Pineau, Joelle, Precup, Doina, and Bengio, Yoshua. Independently controllable features. *arXiv preprint arXiv:1708.01289*, 2017.
- Vedantam, Ramakrishna, Fischer, Ian, Huang, Jonathan, and Murphy, Kevin. Generative models of visually grounded imagination. *International Conference on Learning Representations*, 2018.
- Ver Steeg, Greg and Galstyan, Aram. Maximally informative hierarchical representations of high-dimensional data. In *Artificial Intelligence and Statistics*, pp. 1004–1012, 2015.
- Watanabe, Satoshi. Information theoretical analysis of multivariate correlation. *IBM Journal of research and development*, 4(1):66–82, 1960.
- Zhao, Shengjia, Song, Jiaming, and Ermon, Stefano. Infovae: Information maximizing variational autoencoders. *arXiv preprint arXiv:1706.02262*, 2017.

## Supplementary Materials

### A. Mutual Information Gap

#### A.1 Estimation of $I(z_k; v_k)$

With any inference network  $q(z|x)$ , we can compute the mutual information  $I(z; v)$  by assuming the model  $p(v)p(x|v)q(z|x)$ . Specifically, we compute this for every pair of latent variable  $z_j$  and ground truth factor  $v_k$ .

We make the following assumptions:

- The inference distribution  $q(z_j|x)$  can be sampled from and is known for all  $j$ .
- The generating process  $p(n|v_k)$  can be sampled from and is known.
- Simplifying assumption:  $p(v_k)$  and  $p(n|v_k)$  are quantized (ie. the empirical distributions).

We use the following notation:

- Let  $\mathcal{X}_{v_k}$  be the support of  $p(n|v_k)$ .

Then the mutual information can be estimated as following:

$$\begin{aligned}
 & I(z_j; v_k) \\
 &= \mathbb{E}_{q(z_j, v_k)} [\log q(z_j, v_k) - \log q(z_j) - \log p(v_k)] \\
 &= \mathbb{E}_{q(z_j, v_k)} \left[ \log \sum_{n=1}^N q(z_j, v_k, n) - \log q(z_j) - \log p(v_k) \right] \\
 &= \mathbb{E}_{p(v_k)p(n'|v_k)q(z_j|n')} \left[ \log \sum_{n=1}^N p(v_k)p(n|v_k)q(z_j|n) - \log q(z_j) - \log p(v_k) \right] \tag{S1} \\
 &= \mathbb{E}_{p(v_k)p(n'|v_k)q(z_j|n')} \left[ \log \sum_{n=1}^N \mathbb{1}[n \in \mathcal{X}_{v_k}]p(n|v_k)q(z_j|n) \right] + \mathbb{E}_{q(z_j)} [-\log q(z_j)] \\
 &= \mathbb{E}_{p(v_k)p(n'|v_k)q(z_j|n')} \left[ \log \sum_{n \in \mathcal{X}_{v_k}} q(z_j|n)p(n|v_k) \right] + H(z_j)
 \end{aligned}$$

where the expectation is to make sampling explicit.

To reduce variance, we perform stratified sampling over  $p(v_k)$ , and use 10,000 samples from  $q(n, z_k)$  for each value of  $v_k$ . To estimate  $H(z_j)$  we sample from  $p(n)q(z_j|n)$  and perform stratified sampling over  $p(n)$ . The computation time of our estimation procedure depends on the dataset size but in general can be done in a few minutes for the datasets in our experiments.

#### A.2 Normalization

It is known that when  $v_k$  is discrete, then

$$I(z_j; v_k) = \underbrace{H(v_k)}_{\geq 0} - \underbrace{H(v_k|z_j)}_{\geq 0} \leq H(v_k) \tag{S2}$$

This bound is tight if the model can make  $H(v_k|z_j)$  zero, ie. there exist an invertible function between  $z_j$  and  $v_k$ . On the other hand, if mutual information is not maximal, then we know it is because of a high conditional entropy  $H(v_k|z_j)$ . This suggests our metric is meaningful as it is measuring how much information  $z_j$  retains about  $v_k$  regardless of the parameterization of their distributions.

### B. ELBO TC-Decomposition

Proof of the decomposition in (3):

$$\begin{aligned}
 & \frac{1}{N} \sum_{n=1}^N \mathbf{D}_{\text{KL}}(q(z|x_n)||p(z)) = \mathbb{E}_{p(n)} \left[ \mathbf{D}_{\text{KL}}(q(z|n)||p(z)) \right] \\
 &= \mathbb{E}_{p(n)} \left[ \mathbb{E}_{q(z|n)} \left[ \log q(z|n) - \log p(z) + \log q(z) - \log q(z) + \log \prod_j q(z_j) - \log \prod_j q(z_j) \right] \right] \\
 &= \mathbb{E}_{q(z,n)} \left[ \log \frac{q(z|n)}{q(z)} \right] + \mathbb{E}_{q(z)} \left[ \log \frac{q(z)}{\prod_j q(z_j)} \right] + \mathbb{E}_{q(z)} \left[ \sum_j \log \frac{q(z_j)}{p(z_j)} \right] \\
 &= \mathbb{E}_{q(z,n)} \left[ \log \frac{q(z|n)p(n)}{q(z)p(n)} \right] + \mathbb{E}_{q(z)} \left[ \log \frac{q(z)}{\prod_j q(z_j)} \right] + \sum_j \mathbb{E}_{q(z)} \left[ \log \frac{q(z_j)}{p(z_j)} \right] \\
 &= \mathbb{E}_{q(z,n)} \left[ \log \frac{q(z|n)p(n)}{q(z)p(n)} \right] + \mathbb{E}_{q(z)} \left[ \log \frac{q(z)}{\prod_j q(z_j)} \right] + \sum_j \mathbb{E}_{q(z_j)q(z_{\setminus j})} \left[ \log \frac{q(z_j)}{p(z_j)} \right] \\
 &= \mathbb{E}_{q(z,n)} \left[ \log \frac{q(z|n)p(n)}{q(z)p(n)} \right] + \mathbb{E}_{q(z)} \left[ \log \frac{q(z)}{\prod_j q(z_j)} \right] + \sum_j \mathbb{E}_{q(z_j)} \left[ \log \frac{q(z_j)}{p(z_j)} \right] \\
 &= \underbrace{\mathbf{D}_{\text{KL}}(q(z,n)||q(z)p(n))}_{\text{(i) Index-Code MI}} + \underbrace{\mathbf{D}_{\text{KL}}(q(z)||\prod_j q(z_j))}_{\text{(ii) Total Correlation}} + \underbrace{\sum_j \mathbf{D}_{\text{KL}}(q(z_j)||p(z_j))}_{\text{(iii) Dimension-wise KL}}
 \end{aligned}$$

### B.1 Minibatch Weighted Sampling (MWS)

First, let  $\mathcal{B}_M = \{n_1, \dots, n_M\}$  be a minibatch of  $M$  indices where each element is sampled i.i.d. from  $p(n)$ , so for any sampled batch instance  $\mathcal{B}_M$ ,  $p(\mathcal{B}_M) = (1/N)^M$ . Let  $r(\mathcal{B}_M|n)$  denote the probability of a sampled minibatch where one of the elements is fixed to be  $n$  and the rest are sampled i.i.d. from  $p(n)$ . This gives  $r(x_M|n) = (1/N)^{M-1}$ .

$$\begin{aligned}
 & \mathbb{E}_{q(z)} [\log q(z)] \\
 &= \mathbb{E}_{q(z,n)} [\log \mathbb{E}_{n' \sim p(n)} [q(z|n')]] \\
 &= \mathbb{E}_{q(z,n)} \left[ \log \mathbb{E}_{p(\mathcal{B}_M)} \left[ \frac{1}{M} \sum_{m=1}^M q(z|n_m) \right] \right] \\
 &\geq \mathbb{E}_{q(z,n)} \left[ \log \mathbb{E}_{r(\mathcal{B}_M|n)} \left[ \frac{p(\mathcal{B}_M)}{r(\mathcal{B}_M|n)} \frac{1}{M} \sum_{m=1}^M q(z|n_m) \right] \right] \\
 &= \mathbb{E}_{q(z,n)} \left[ \log \mathbb{E}_{r(\mathcal{B}_M|n)} \left[ \frac{1}{NM} \sum_{m=1}^M q(z|n_m) \right] \right]
 \end{aligned} \tag{S3}$$

The inequality is due to  $r$  having a support that is a subset of that of  $p$ . During training, when provided with a minibatch of samples  $\{n_1, \dots, n_M\}$ , we can use the estimator

$$\mathbb{E}_{q(z)} [\log q(z)] \approx \frac{1}{M} \sum_{i=1}^M \left[ \log \sum_{j=1}^M q(z(n_i)|n_j) - \log(NM) \right] \tag{S4}$$

where  $z(n_i)$  is a sample from  $q(z|n_i)$ .

### B.2 Minibatch Stratified Sampling (MSS)

In this setting, we sample a minibatch of indices  $\mathcal{B}_M = \{n_1, \dots, n_M\}$  to estimate  $q(z)$  for some  $z$  that was originally sampled from  $q(z|n^*)$  for a particular index  $n^*$ . We define  $p(\mathcal{B}_M)$  to be uniform over all minibatches of size  $M$ . To sample

from  $p(B_M)$ , we sample  $M$  indices from  $\{1, \dots, N\}$  **without replacement**. Then the following expressions hold:

$$\begin{aligned}
 q(z) &= \mathbb{E}_{p(n)}[q(z|n)] \\
 &= \mathbb{E}_{p(B_M)} \left[ \frac{1}{M} \sum_{m=1}^M q(z|n_m) \right] \\
 &= \mathbb{P}(n^* \in B_M) \mathbb{E} \left[ \frac{1}{M} \sum_{m=1}^M q(z|n_m) \middle| n^* \in B_M \right] + \mathbb{P}(n^* \notin B_M) \mathbb{E} \left[ \frac{1}{M} \sum_{m=1}^M q(z|n_m) \middle| n^* \notin B_M \right] \\
 &= \frac{M}{N} \mathbb{E} \left[ \frac{1}{M} \sum_{m=1}^M q(z|n_m) \middle| n^* \in B_M \right] + \frac{N-M}{N} \mathbb{E} \left[ \frac{1}{M} \sum_{m=1}^M q(z|n_m) \middle| n^* \notin B_M \right]
 \end{aligned} \tag{S5}$$

During training, we sample a minibatch of size  $M$  without replacement **that does not contain**  $n^*$ . We estimate the first term using  $n^*$  and  $M-1$  other samples, and the second term using the  $M$  samples that are not  $n^*$ . One can also view this as sampling a minibatch of size  $M+1$  where  $n^*$  is one of the elements, and let  $B_{M+1} \setminus \{n^*\} = \hat{B}_M = \{n_1, \dots, n_M\}$  be the elements that are not equal to  $n^*$ , then we can estimate the first expectation using  $\{n^*\} \cup \{n_1, \dots, n_{M-1}\}$  and the second expectation using  $\{n_1, \dots, n_M\}$ . This estimator can be written as:

$$q(z) \approx f(z, n^*, \hat{B}_M) = \frac{1}{N} q(z|n^*) + \frac{1}{M} \sum_{m=1}^{M-1} q(z|n_m) + \frac{N-M}{NM} q(z|n_M) \tag{S6}$$

which is unbiased, and exact if  $M = N$ .

### B.2.1 STOCHASTIC ESTIMATION

During training, we estimate each term of the decomposed ELBO,  $\log p(x|z)$ ,  $\log p(z)$ ,  $\log q(z|x)$ ,  $\log q(z)$ , and  $\log \prod_{j=1}^K q(z_j)$ , where the last two terms are estimated using MSS. For convenience, we use the same minibatch that was used to sample  $z$  to estimate these two terms.

$$\mathbb{E}_{q(z,n)}[\log q(z)] \approx \frac{1}{M+1} \sum_{i=1}^{M+1} \log f(z_i, n_i, B_{M+1} \setminus \{n_i\}) \tag{S7}$$

Note that this estimator is a lower bound on  $\mathbb{E}_{q(z)}[\log q(z)]$  due to Jensen's inequality,

$$\begin{aligned}
 &\mathbb{E}_{p(B_{M+1})} \left[ \frac{1}{M+1} \sum_{i=1}^{M+1} \log f(z_i, n_i, B_{M+1} \setminus \{n_i\}) \right] \\
 &= \mathbb{E}_{p(B_{M+1})} [\log f(z_i, n_i, B_{M+1} \setminus \{n_i\})] \\
 &\leq \log \mathbb{E}_{p(B_{M+1})} [f(z_i, n_i, B_{M+1} \setminus \{n_i\})] \\
 &= \mathbb{E}_{q(z)} [\log q(z)]
 \end{aligned} \tag{S8}$$

However, the bias goes to zero if  $M$  increases and the equality holds if  $M = N$ . (Note that this is in terms of the empirical distribution  $p(n)$  used in our decomposition rather than the unknown data distribution.)

### B.2.2 EXPERIMENTS

While MSS is an unbiased estimator of  $q(z)$ , MWS is not. Moreover, neither of them is unbiased for estimating  $\log q(z)$  due to Jensen's inequality. Take MSS as an example:

$$\mathbb{E}_{p(n)} [\log MSS(z)] \leq \log \mathbb{E}_{p(n)} [MSS(z)] = \log q(z) \tag{S9}$$

We observe from preliminary experiments that using MSS results in performance similar to MWS.

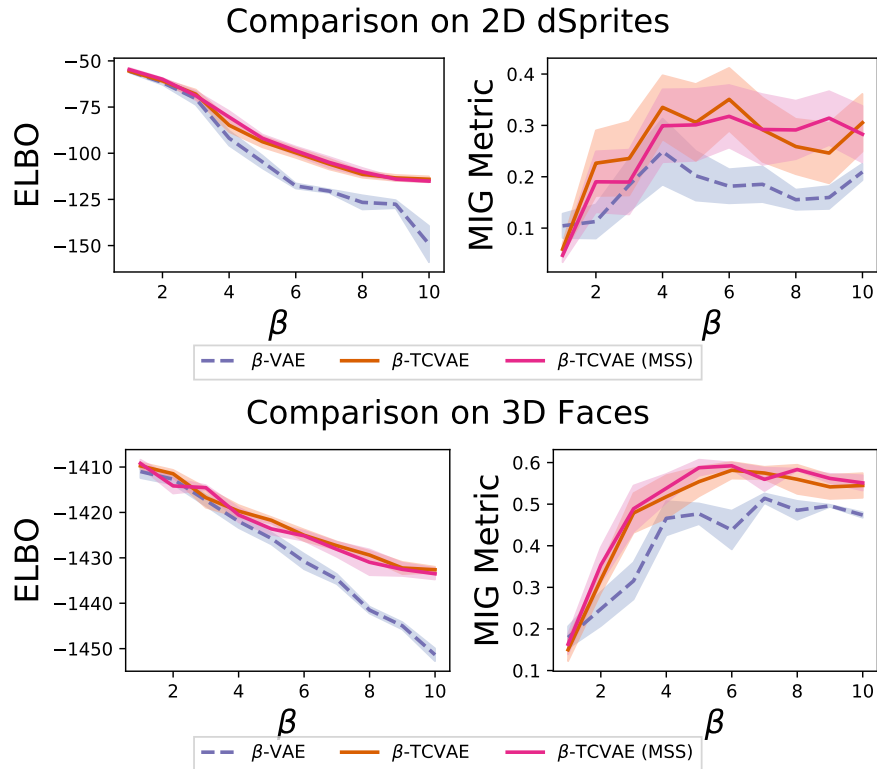


Figure S1. MSS performs similarly to MWS.

## C. Extra Ablation Experiments

We performed some ablation experiments using slight variants of  $\beta$ -TCVAE, but found no significant meaningful differences.

### C.1 Removing Index-code MI ( $\alpha = 0$ )

We show some preliminary experiments using  $\alpha = 0$  in (5). By removing the penalty on index-code MI, the autoencoder can then place as much information as necessary into the latent variables. However, we find no significant difference between setting  $\alpha$  to 0 or to 1, and the setting is likely empirically dataset-dependent. Further experiments use  $\alpha = 1$  so that it is a proper lower bound on  $\log p(x)$  and to avoid the extensive hyperparameter tuning of having to choose  $\alpha$ . Note that works claiming better representations can be obtained with low  $\alpha$  (Chen et al., 2016; Makhzani et al., 2016) and moderate  $\alpha$  (Achille & Soatto, 2017) both exist.

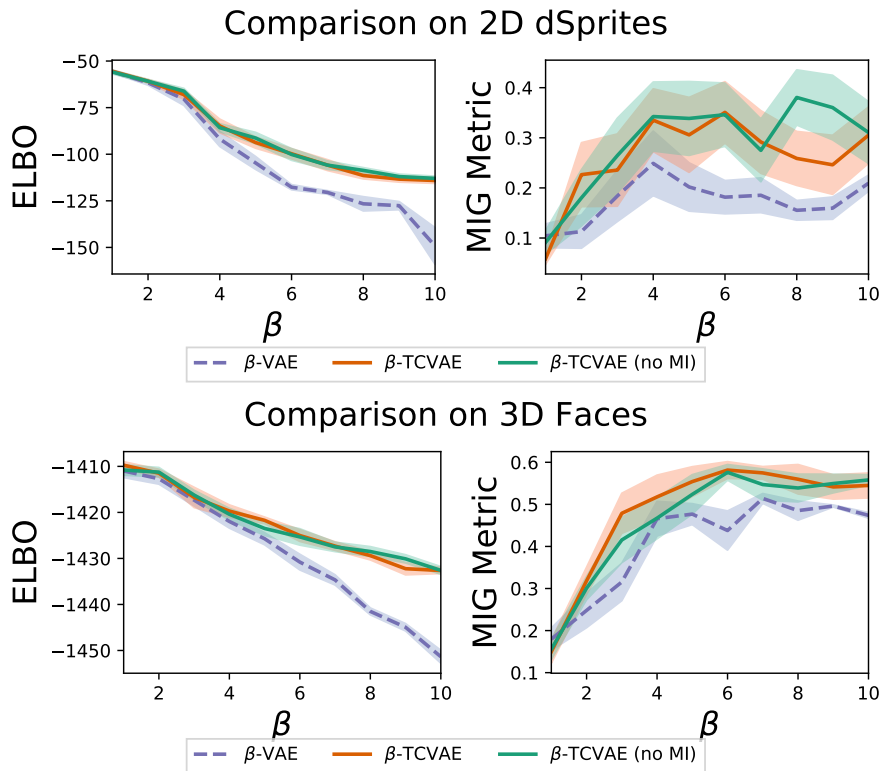


Figure S2. ELBO vs. Disentanglement plots showing  $\beta$ -TCVAE (5) but with  $\alpha$  set to 0.

## C.2 Factorial Normalizing Flow

We also performed experiments with a factorial normalizing flow (FNF) as a flexible prior. Using a flexible prior is conceptually similar to ignoring the dimension-wise KL term in (3) (ie.  $\gamma = 0$  in (5)), but empirically the slow updates for the normalizing flow should help stabilize the aggregate posterior. Each dimension is a normalizing flow of depth 32, and the parameters are trained to maximize the  $\beta$ -TCVAE objective. The FNF can fit multi-modal distributions. From our preliminary experiments, we found no significant improvement from using a factorial Gaussian prior and so decided not to include this in the paper.



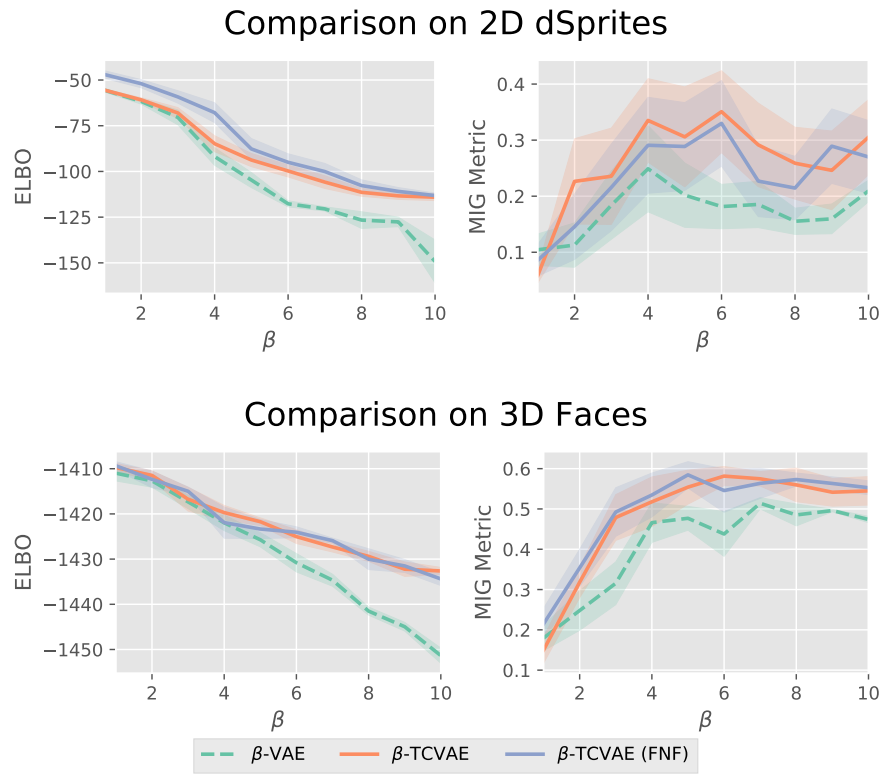


Figure S3. ELBO vs. Disentanglement plots showing the  $\beta$ -TCVAE with a factorial normalizing flow (FNF).

## D. Comparison of Best Models

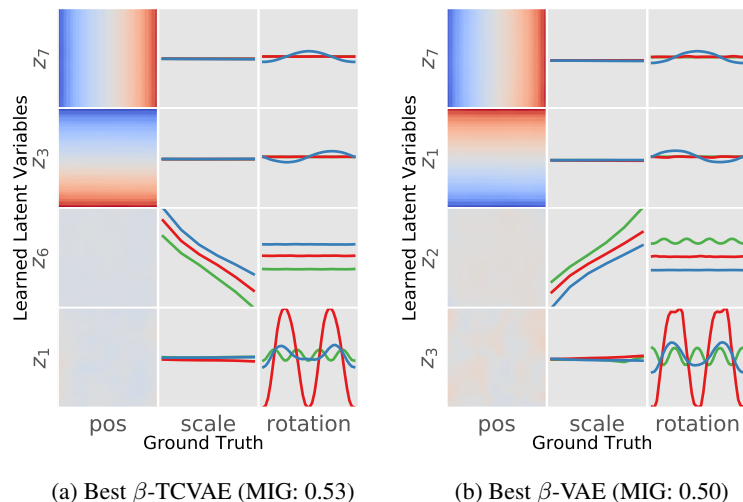


Figure S4. **MIG is able to capture subtle differences.** Relation between the learned variables and the ground truth factors are plotted for the best  $\beta$ -TCVAE and  $\beta$ -VAE on the dSprites dataset according to the MIG metric are shown. Each row corresponds to a ground truth factor and each column to a latent variable. The plots show the relationship between the latent variable mean versus the ground truth factor, with only active latent variables shown. For position, a color of blue indicates a high value and red indicates a low value. The colored lines indicate object shape with red being oval, green being square, and blue being heart. Interestingly, the latent variables for rotation has 2 peaks for oval and 4 peaks for square, suggesting that the models have produced a more compact code by observing that the object is rendered the same for certain degrees of rotation.

## E. Invariance to Hyperparameters

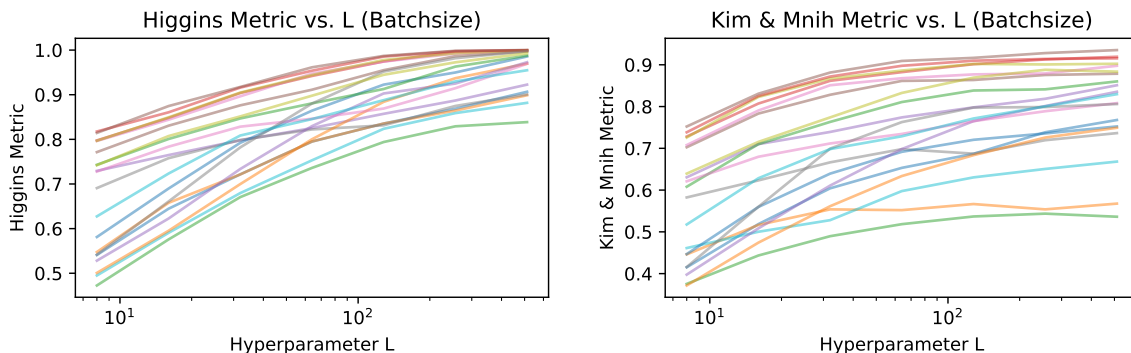


Figure S5. The distribution of each classifier-based metric is shown to be extremely dependent on the hyperparameter  $L$ . Each colored line is a different VAE trained with the unmodified ELBO objective.

We believe that a metric should also be invariant to any hyperparameters. For instance, the existence of hyperparameters in the prior metrics means that a different set of hyperparameter values can result in different metric outputs. Additionally, even with a stable classifier that always outputs the same accuracy for a given dataset, the creation of a dataset for classifier-based metrics can still be problematic.

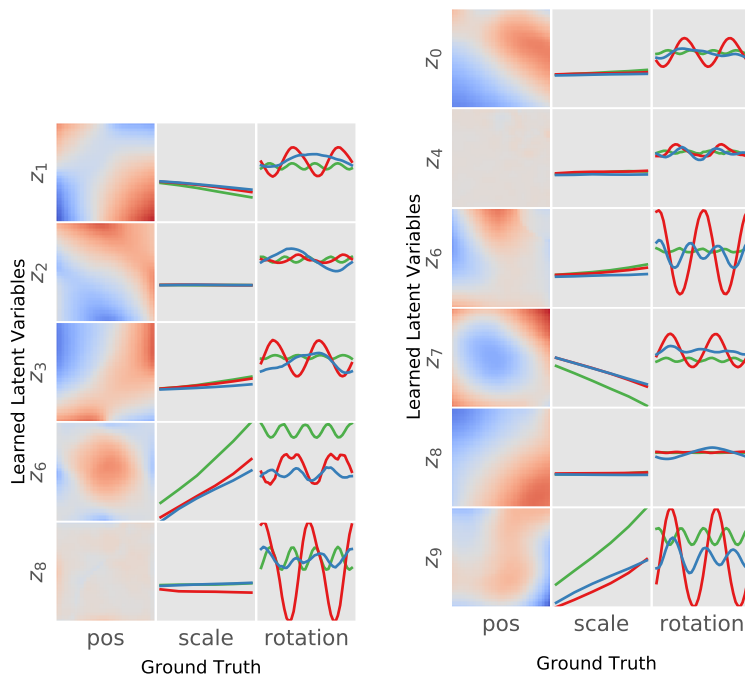
The aggregated inputs used by [Higgins et al. \(2017\)](#) and [Kim & Mnih \(2018\)](#) depend on a batch size  $L$  that is difficult to tune and leads to inconsistent metric values. In fact, we empirically find that these metrics are most informative with a small

$L$ . Figure S5 plots the Higgins et al. (2017) metric against  $L$  for 20 fully trained VAEs. As  $L$  increases, the aggregated inputs become more quantized. Not only does this increase the accuracy of the metric, but it also *reduces the gap between models*, making it hard to discriminate similarly performing models. The relative ordering of models is also not preserved with different values.

### F. MIG Traversal

To give some insight into what MIG is capturing, we show some  $\beta$ -TCVAE experiments with scores near quantized values of MIG. In general, we find that MIG gives low scores to entangled representations when even just two variables are not axis-aligned. We find that MIG shows a clearer pattern for scoring position and scale, but less so for rotation. This is likely due to latent variables having a low MI with rotation. In an unsupervised setting, certain ground truth rotation values are impossible to differentiate (e.g. 0 and 180 for ovals and squares), so the latent variable simply learns to map these to the same value. This is evident in the plots where latent variables describing rotation are many-to-one. The existence of factors with redundant values may be one downside to using MIG as a scoring mechanism, but such factors only appear in simple datasets such as dSprites.

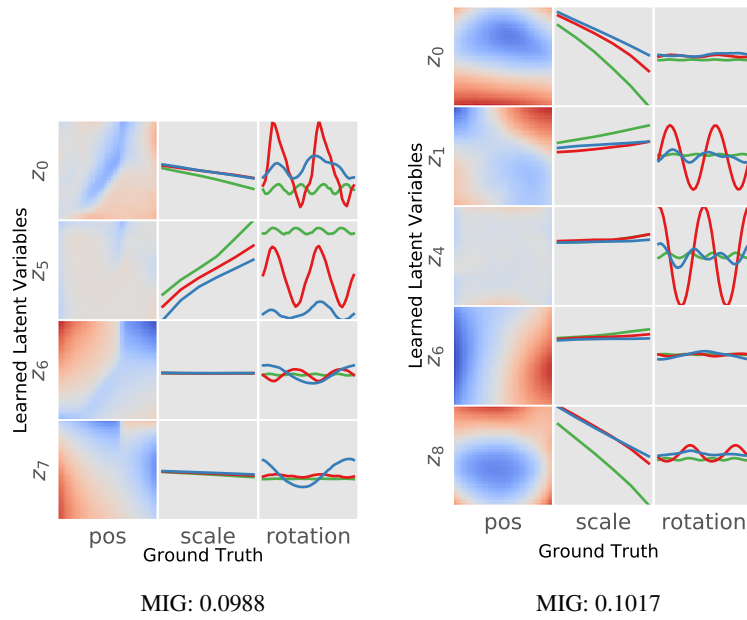
Note that this type of plot does not show the whole picture. Specifically, only the mean of the latent variables is shown, while the uncertainty of the latent variables is not. Mutual information computes the reduction in uncertainty after observing one factor, so the uncertainty is important but cannot be easily plotted. Some changes in MIG may be explained by a reduction in the uncertainty even though the plots may look similar.



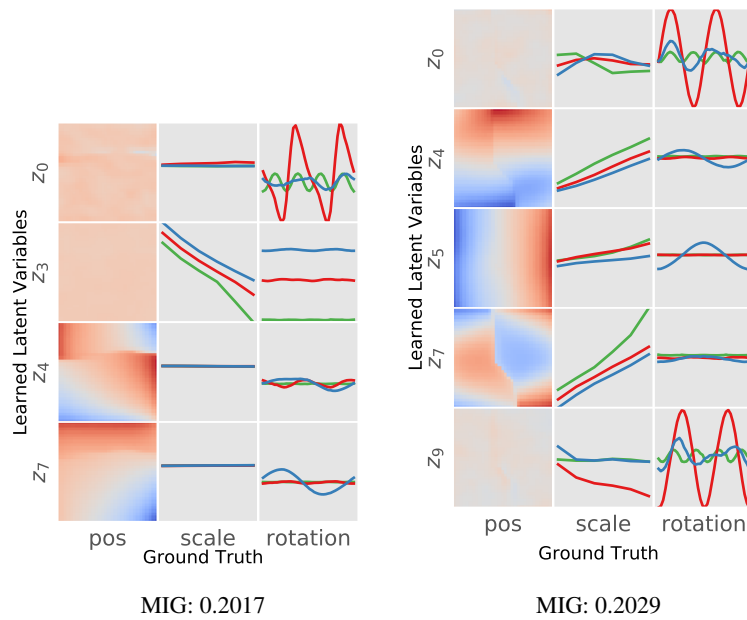
MIG: 0.0169

MIG: 0.0214

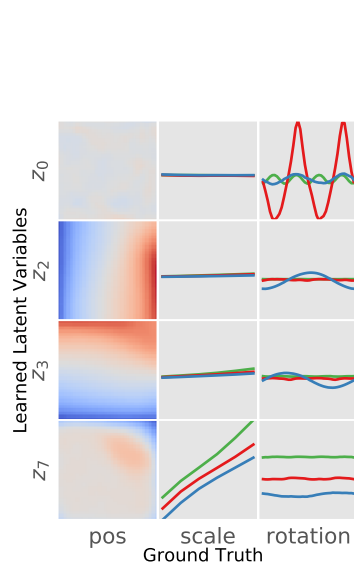
**Score near 0.0.** Representations are extremely entangled.



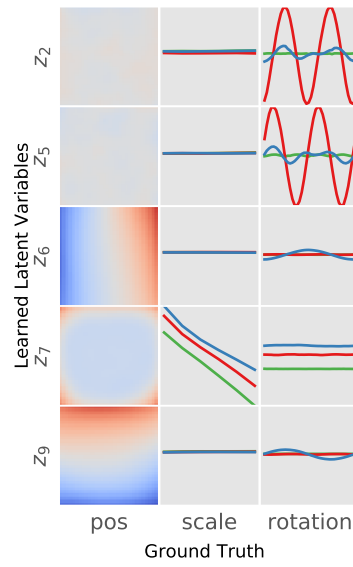
**Score near 0.1.** Representations are less entangled but fail to satisfy axis-alignment.



**Score near 0.2.** Representations are still entangled, but some form is appearing.

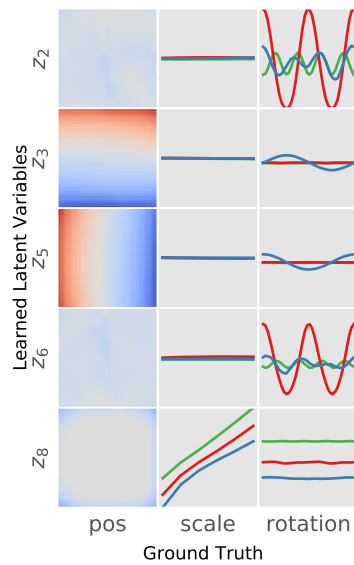


MIG: 0.3155

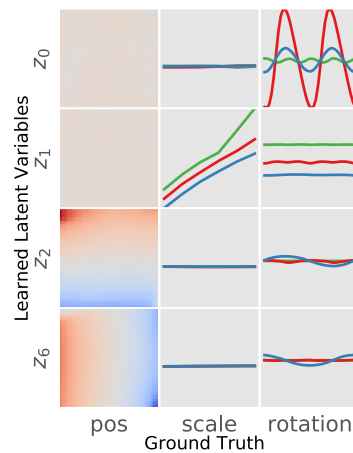


MIG: 0.3271

**Score near 0.3.** Representations look much more disentangled, with some nuances not being completely disentangled.

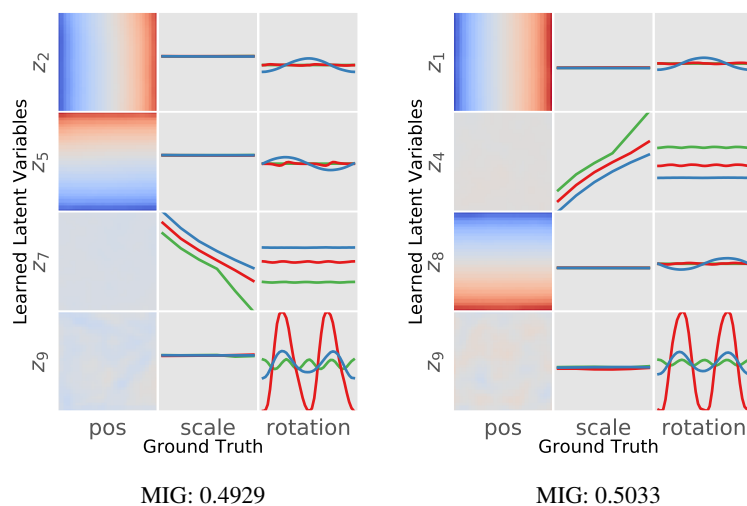


MIG: 0.4092



MIG: 0.4179

**Score near 0.4.** Representations appear to be axis-aligned but rotation is still entangled and position is not perfect.



**Score near 0.5.** Representations appear to be axis-aligned and disentangled. Higher scores are likely reducing entropy (with latent variables appearing closer to a Dirac delta.) To fully match the ground truth, the latent variables would have to be a mixture of Dirac deltas, but such variables would have a high dimension-wise KL with a factorized Gaussian.

### G. Disagreements Between Metrics

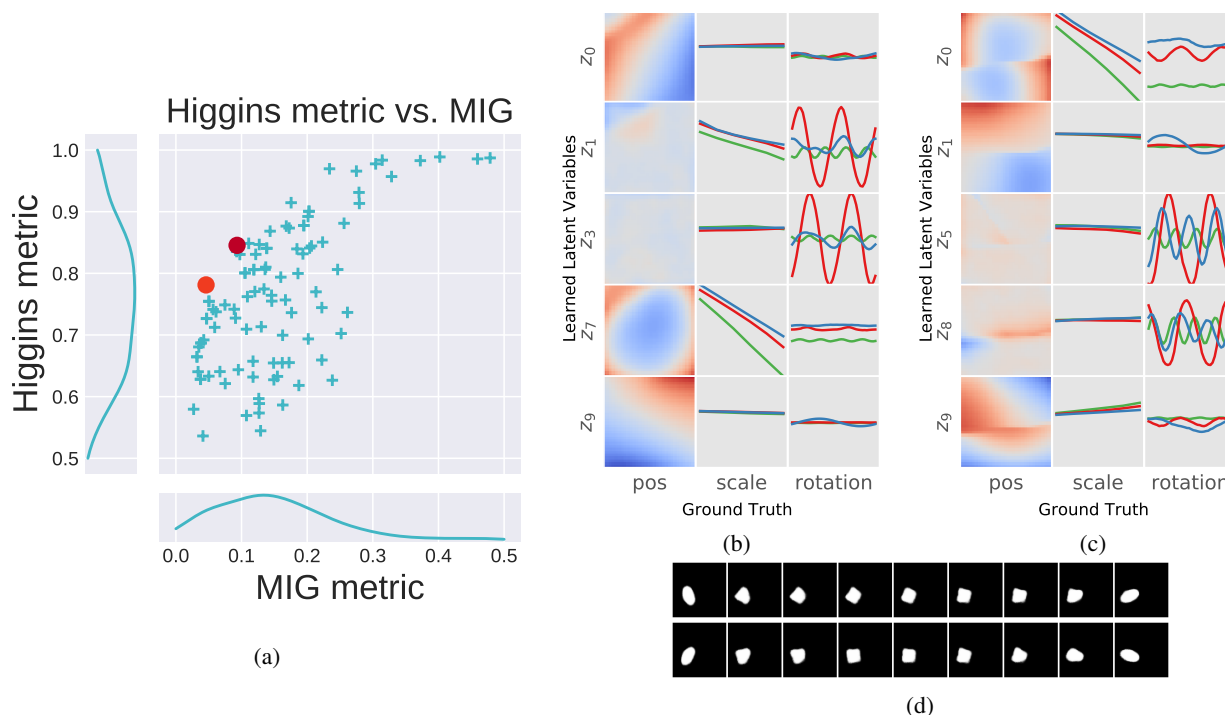


**Figure S12. Entangled representations can have a relatively high Higgins metric while MIG correctly scores it low.** (a) The Higgins metric tends to be overly optimistic compared to the MIG metric. (b, c) Relationships between the ground truth factors and the learned latent variables are shown for the top two controversial models, which are shown as red dots. Each colored line indicates a different shape (see Supplementary Materials). (d) Sample traversals for the two latent variables in model (b) that both depend on rotation, which clearly mirror each other.

Before using the MIG metric, we first show that it is in some ways superior to the Higgins et al. (2017) metric. To find differences between these two metrics, we train 200 models of  $\beta$ -VAE with varying  $\beta$  and different initializations.

Figure S12a shows each model as a single point based on the two metrics. In general, both metrics agree on the most disentangled models; however, the MIG metric falls off very quickly comparatively. In fact, the Higgins metric tends to output an inflated score due to its inability to detect subtle differences and a lack of axis-alignment.

As an example, we can look at controversial models that are disagreed upon by the two metrics (Figure S12b). The most controversial model is shown in Figure S12a as a red dot. While the MIG metric only ranks this model as better than 26% of the models, the Higgins metric ranks it as better than 75% of the models. By inspecting the relationship between the latent units and ground truth factors, we see that only the scale factor seems to be disentangled (Figure S12b). The position factors are not axis aligned, and there are two latent variables for rotation that appear to mirror each other with only a very slight difference. The two rows in Figure S12d show traversals corresponding to the two latent variables for rotation. We see clearly that they simply rotate in the opposite direction. Since the Higgins metric does not enforce that only a single latent variable should influence each factor, it mistakenly assigns a higher disentanglement score to this model. We note that many models near the red dot in the figure exhibit similar behavior.

### G.1 More Controversial Models

Each model can be ordered by either metric (MIG or Higgins) such that each model is assigned a unique integer 1 – 200. We define the most controversial model as  $\max_{\alpha} R(\alpha; Higgins) - R(\alpha; MIG)$ , where a higher rank implies more disentanglement. These are models that the Higgins metric believes to be highly disentangled while MIG believes they are not. Figure S14 shows the top 5 most controversial models.

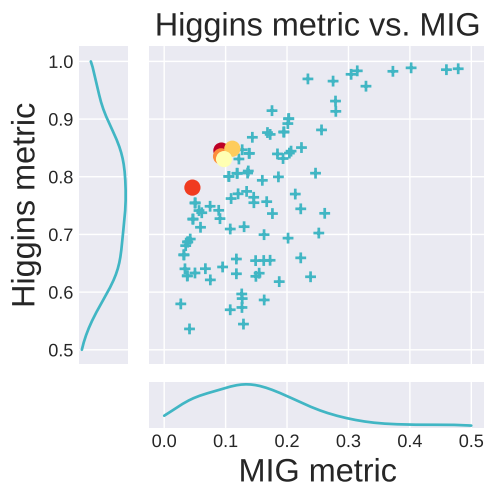


Figure S13. Models as colored dots are those shown in Figure S14.

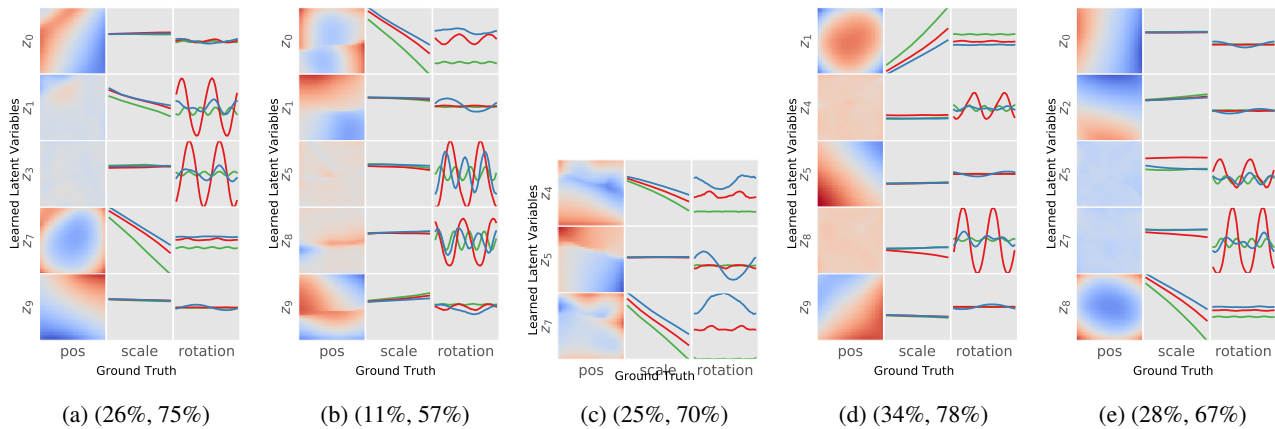


Figure S14. (a-e) The top 5 most controversial models. The brackets indicate the rank of models by MIG and the Higgins metric. For instance, the most controversial model shown in (a) is ranked as better than 75% of model by the Higgins metric, but MIG believes that it is only better than 25% of models.

## H. Training Hyperparameters

Hyperparameters not mentioned are PyTorch v0.2.0 defaults.

**$\beta$ -VAE and  $\beta$ -TCVAE** We used Adam (Kingma & Ba, 2015) with learning rate 0.001. We use a batch size of 2048 for dSprites, 3D faces, and 3D chairs. We use a batch size of 1000 for CelebA.

**InfoGAN** Other than architecture, we used same configuration as DCGAN (Radford et al., 2015).

### H.1 Architectures (PyTorch)

**dSprites** (excluding InfoGAN)

```
class MLPDecoder(nn.Module):
    def __init__(self, output_dim):
        super(MLPDecoder, self).__init__()
        self.output_dim = output_dim
        self.fc1 = nn.Linear(4096, 1200)
        self.fc2 = nn.Linear(1200, 1200)
        self.fc3 = nn.Linear(1200, output_dim)
        self.act = nn.ReLU(inplace=True)

    def forward(self, x):
        h = x.view(-1, 64 * 64)
        h = self.act(self.fc1(h))
        h = self.act(self.fc2(h))
        h = self.fc3(h)
        z = h.view(x.size(0), self.output_dim)
        return z

class MLPDecoder(nn.Module):
    def __init__(self, input_dim):
        super(MLPDecoder, self).__init__()
        self.net = nn.Sequential(
```



```

        nn.Linear(input_dim, 1200),
        nn.Tanh(),
        nn.Linear(1200, 1200),
        nn.Tanh(),
        nn.Linear(1200, 1200),
        nn.Tanh(),
        nn.Linear(1200, 4096)
    )

    def forward(self, z):
        h = z.view(z.size(0), -1)
        h = self.net(h)
        mu_img = h.view(z.size(0), 1, 64, 64)
        return mu_img

```

### 3D Faces and 3D Chairs (except InfoGAN)

```

class ConvEncoder(nn.Module):
    def __init__(self, output_dim):
        super(ConvEncoder, self).__init__()
        self.output_dim = output_dim
        self.conv1 = nn.Conv2d(1, 32, 4, 2, 1) # 32 x 32
        self.bn1 = nn.BatchNorm2d(32)
        self.conv2 = nn.Conv2d(32, 32, 4, 2, 1) # 16 x 16
        self.bn2 = nn.BatchNorm2d(32)
        self.conv3 = nn.Conv2d(32, 64, 4, 2, 1) # 8 x 8
        self.bn3 = nn.BatchNorm2d(64)
        self.conv4 = nn.Conv2d(64, 64, 4, 2, 1) # 4 x 4
        self.bn4 = nn.BatchNorm2d(64)
        self.conv5 = nn.Conv2d(64, 512, 4)
        self.bn5 = nn.BatchNorm2d(512)
        self.conv_z = nn.Conv2d(512, output_dim, 1)
        self.act = nn.ReLU(inplace=True)

    def forward(self, x):
        h = x.view(-1, 1, 64, 64)
        h = self.act(self.bn1(self.conv1(h)))
        h = self.act(self.bn2(self.conv2(h)))
        h = self.act(self.bn3(self.conv3(h)))
        h = self.act(self.bn4(self.conv4(h)))
        h = self.act(self.bn5(self.conv5(h)))
        z = self.conv_z(h).view(x.size(0), self.output_dim)
        return z

class ConvDecoder(nn.Module):
    def __init__(self, input_dim):
        super(ConvDecoder, self).__init__()
        self.conv1 = nn.ConvTranspose2d(input_dim, 512, 1, 1, 0) # 1 x 1
        self.bn1 = nn.BatchNorm2d(512)
        self.conv2 = nn.ConvTranspose2d(512, 64, 4, 1, 0) # 4 x 4
        self.bn2 = nn.BatchNorm2d(64)
        self.conv3 = nn.ConvTranspose2d(64, 64, 4, 2, 1) # 8 x 8
        self.bn3 = nn.BatchNorm2d(64)
        self.conv4 = nn.ConvTranspose2d(64, 32, 4, 2, 1) # 16 x 16

```

```
self.bn4 = nn.BatchNorm2d(32)
self.conv5 = nn.ConvTranspose2d(32, 32, 4, 2, 1) # 32 x 32
self.bn5 = nn.BatchNorm2d(32)
self.conv_final = nn.ConvTranspose2d(32, 1, 4, 2, 1)
self.act = nn.ReLU(inplace=True)

def forward(self, z):
    h = z.view(z.size(0), z.size(1), 1, 1)
    h = self.act(self.bn1(self.conv1(h)))
    h = self.act(self.bn2(self.conv2(h)))
    h = self.act(self.bn3(self.conv3(h)))
    h = self.act(self.bn4(self.conv4(h)))
    h = self.act(self.bn5(self.conv5(h)))
    mu_img = self.conv_final(h)
    return mu_img
```

## InfoGAN

```
class ConvEncoder(nn.Module):
    def __init__(self, output_dim):
        super(ConvEncoder, self).__init__()
        self.output_dim = output_dim

        self.conv1 = nn.Conv2d(1, 32, 4, 2, 1) # 32 x 32
        self.bn1 = nn.BatchNorm2d(32)
        self.conv2 = nn.Conv2d(32, 32, 4, 2, 1) # 16 x 16
        self.bn2 = nn.BatchNorm2d(32)
        self.conv3 = nn.Conv2d(32, 64, 4, 2, 1) # 8 x 8
        self.bn3 = nn.BatchNorm2d(64)
        self.conv4 = nn.Conv2d(64, 64, 4, 2, 1) # 4 x 4
        self.bn4 = nn.BatchNorm2d(64)
        self.conv5 = nn.Conv2d(64, 512, 4)
        self.bn5 = nn.BatchNorm2d(512)
        self.conv_z = nn.Conv2d(512, output_dim, 1)
        self.conv_d = nn.Conv2d(512, 1, 1)
        self.act = nn.LeakyReLU(0.2, inplace=True)

    def forward(self, x):
        return self.recognition(x)

    def discriminate(self, x):
        h = x.view(-1, 1, 64, 64)
        h = self.act(self.bn1(self.conv1(h)))
        h = self.act(self.bn2(self.conv2(h)))
        h = self.act(self.bn3(self.conv3(h)))
        h = self.act(self.bn4(self.conv4(h)))
        h = self.act(self.bn5(self.conv5(h)))
        d = self.conv_d(h).view(x.size(0), 1)
        return d

    def recognition(self, x):
        h = x.view(-1, 1, 64, 64)
        h = self.act(self.bn1(self.conv1(h)))
        h = self.act(self.bn2(self.conv2(h)))
```

```

h = self.act(self.bn3(self.conv3(h)))
h = self.act(self.bn4(self.conv4(h)))
h = self.act(self.bn5(self.conv5(h)))
z = self.conv_z(h).view(x.size(0), self.output_dim)
return z

```

```

class ConvDecoder(nn.Module):
    def __init__(self, input_dim):
        super(ConvDecoder, self).__init__()
        self.conv1 = nn.ConvTranspose2d(input_dim, 512, 1, 1, 0) # 1 x 1
        self.bn1 = nn.BatchNorm2d(512)
        self.conv2 = nn.ConvTranspose2d(512, 64, 4, 1, 0) # 4 x 4
        self.bn2 = nn.BatchNorm2d(64)
        self.conv3 = nn.ConvTranspose2d(64, 64, 4, 2, 1) # 8 x 8
        self.bn3 = nn.BatchNorm2d(64)
        self.conv4 = nn.ConvTranspose2d(64, 32, 4, 2, 1) # 16 x 16
        self.bn4 = nn.BatchNorm2d(32)
        self.conv5 = nn.ConvTranspose2d(32, 32, 4, 2, 1) # 32 x 32
        self.bn5 = nn.BatchNorm2d(32)
        self.conv_final = nn.ConvTranspose2d(32, 1, 4, 2, 1)
        self.act = nn.LeakyReLU(0.2, inplace=True)

    def forward(self, z):
        h = z.view(z.size(0), z.size(1), 1, 1)
        h = self.act(self.bn1(self.conv1(h)))
        h = self.act(self.bn2(self.conv2(h)))
        h = self.act(self.bn3(self.conv3(h)))
        h = self.act(self.bn4(self.conv4(h)))
        h = self.act(self.bn5(self.conv5(h)))
        mu_img = self.conv_final(h)
        return mu_img

```

## CelebA

```

class ConvEncoder(nn.Module):
    def __init__(self, output_dim):
        super(ConvEncoder, self).__init__()
        self.output_dim = output_dim
        self.conv1 = nn.Conv2d(3, 64, 4, 2, 1) # 32 x 32
        self.bn1 = nn.BatchNorm2d(64)
        self.conv2 = nn.Conv2d(64, 128, 4, 2, 1) # 16 x 16
        self.bn2 = nn.BatchNorm2d(128)
        self.conv3 = nn.Conv2d(128, 128, 4, 2, 1) # 8 x 8
        self.bn3 = nn.BatchNorm2d(128)
        self.conv4 = nn.Conv2d(128, 256, 4, 2, 1) # 4 x 4
        self.bn4 = nn.BatchNorm2d(256)
        self.conv5 = nn.Conv2d(256, 512, 4)
        self.bn5 = nn.BatchNorm2d(512)
        self.conv_z = nn.Conv2d(512, output_dim, 1)
        self.act = nn.ReLU(inplace=True)

    def forward(self, x):

```

```

h = x.view(-1, 3, IMG_SIZE, IMG_SIZE)
h = self.act(self.bn1(self.conv1(h)))
h = self.act(self.bn2(self.conv2(h)))
h = self.act(self.bn3(self.conv3(h)))
h = self.act(self.bn4(self.conv4(h)))
h = self.act(self.bn5(self.conv5(h)))
z = self.conv_z(h).view(x.size(0), self.output_dim)
return z

class ConvDecoder(nn.Module):
    def __init__(self, input_dim):
        super(ConvDecoder, self).__init__()
        self.conv1 = nn.ConvTranspose2d(input_dim, 512, 1, 1, 0) # 1 x 1
        self.bn1 = nn.BatchNorm2d(512)
        self.conv2 = nn.ConvTranspose2d(512, 256, 4, 1, 0) # 4 x 4
        self.bn2 = nn.BatchNorm2d(256)
        self.conv3 = nn.ConvTranspose2d(256, 128, 4, 2, 1) # 8 x 8
        self.bn3 = nn.BatchNorm2d(128)
        self.conv4 = nn.ConvTranspose2d(128, 128, 4, 2, 1) # 16 x 16
        self.bn4 = nn.BatchNorm2d(128)
        self.conv5 = nn.ConvTranspose2d(128, 64, 4, 2, 1) # 32 x 32
        self.bn5 = nn.BatchNorm2d(64)
        self.conv_final_mu = nn.ConvTranspose2d(64, 3, 4, 2, 1)
        self.act = nn.ReLU(inplace=True)

    def forward(self, z):
        batchsize = z.size(0)
        h = z.view(batchsize, -1, 1, 1)
        h = self.act(self.bn1(self.conv1(h)))
        h = self.act(self.bn2(self.conv2(h)))
        h = self.act(self.bn3(self.conv3(h)))
        h = self.act(self.bn4(self.conv4(h)))
        h = self.act(self.bn5(self.conv5(h)))
        img_mu = self.conv_final_mu(h).view(batchsize, 3, 64, 64).sigmoid()
        return img_mu

```

## H.2 Effect of Batchsize

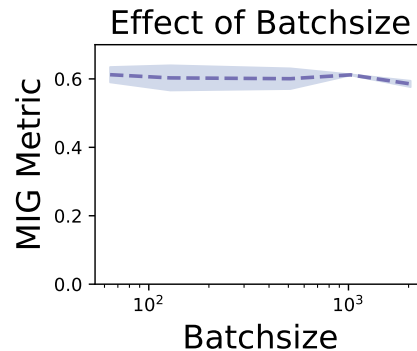


Figure S15. We use a high batchsize to account for the bias in minibatch estimation. However, we find that lower batchsizes are still effective when using  $\beta$ -TCVAE, suggesting that a high batchsize may not be necessary. This is run on the 3D faces dataset with  $\beta=6$ .

## I. Random Samples

### I.1 Real Samples

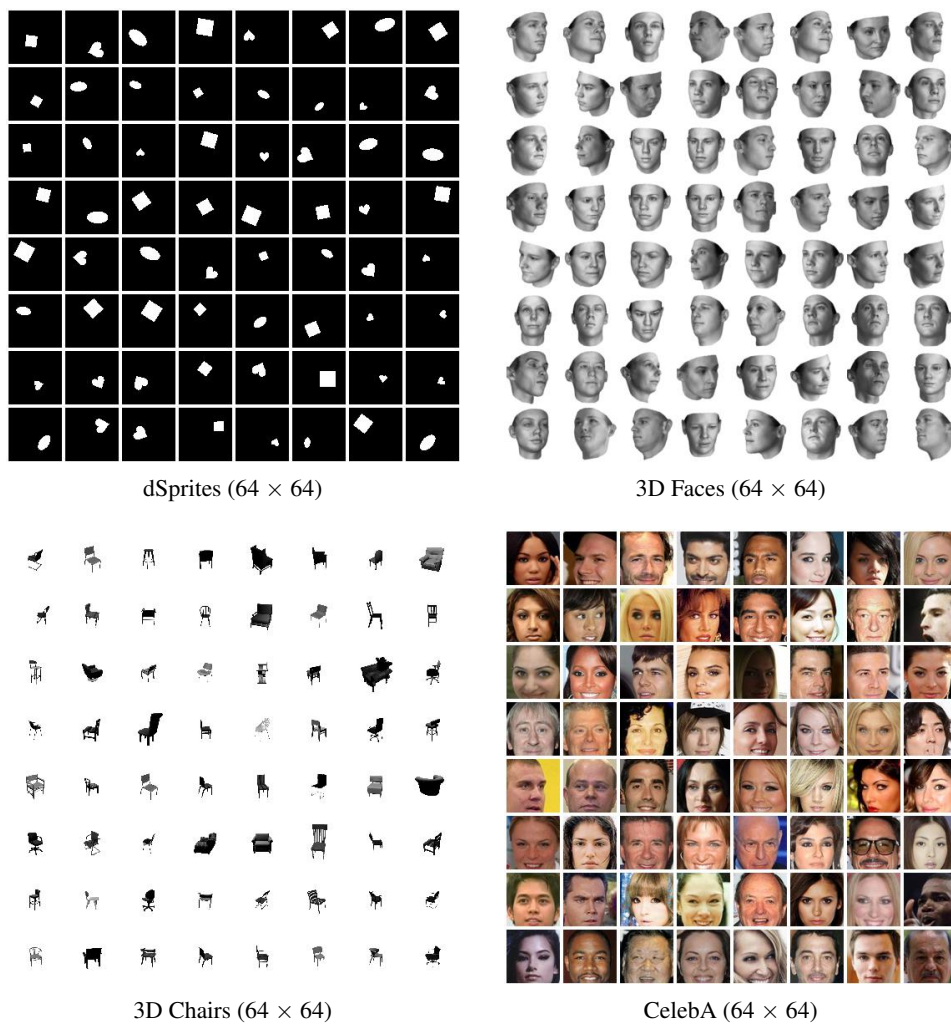


Figure S16. Real samples from the training data set.

## I.2 Latent Traversals

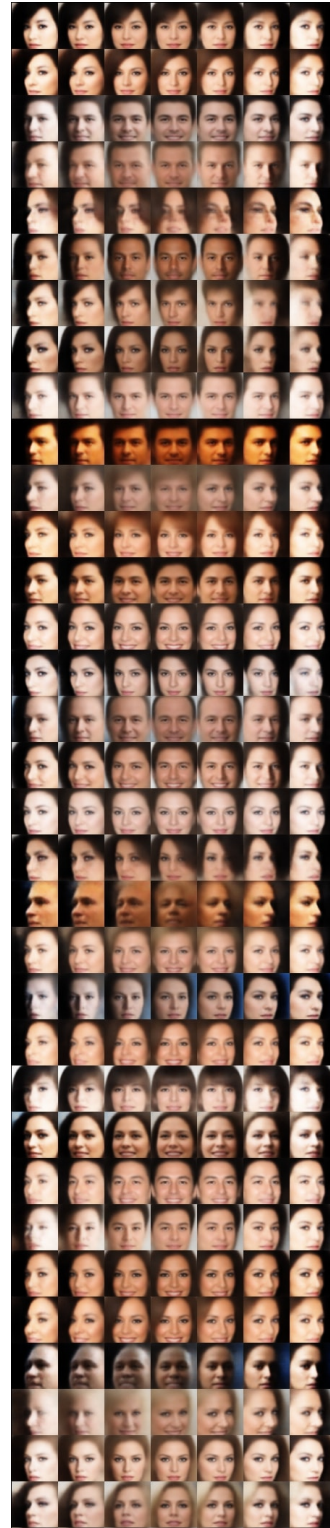
$\beta$ -TCVAE MODEL ONE ( $\beta=15$ )



Baldness



Dramatic masculinity



Azimuth

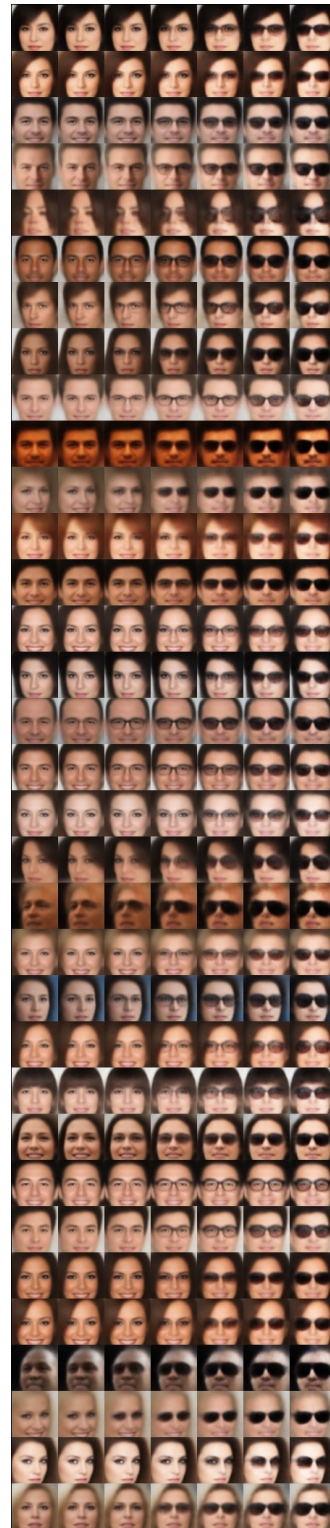
Isolating Sources of Disentanglement in Variational Autoencoders



Contrast



Mustache (shared with Glasses)



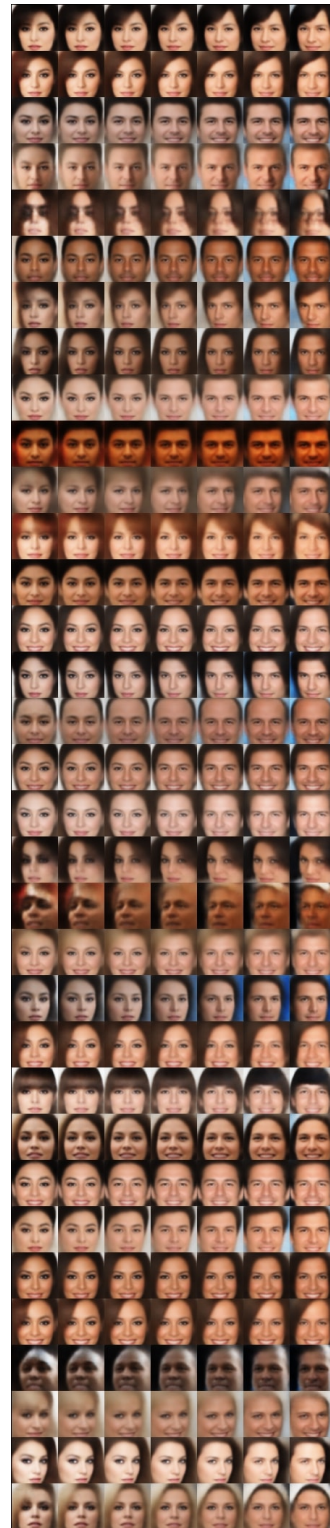
Glasses (shared with Mustache)



Smile (shared with Shadow)



Shadow (shared with Smile)



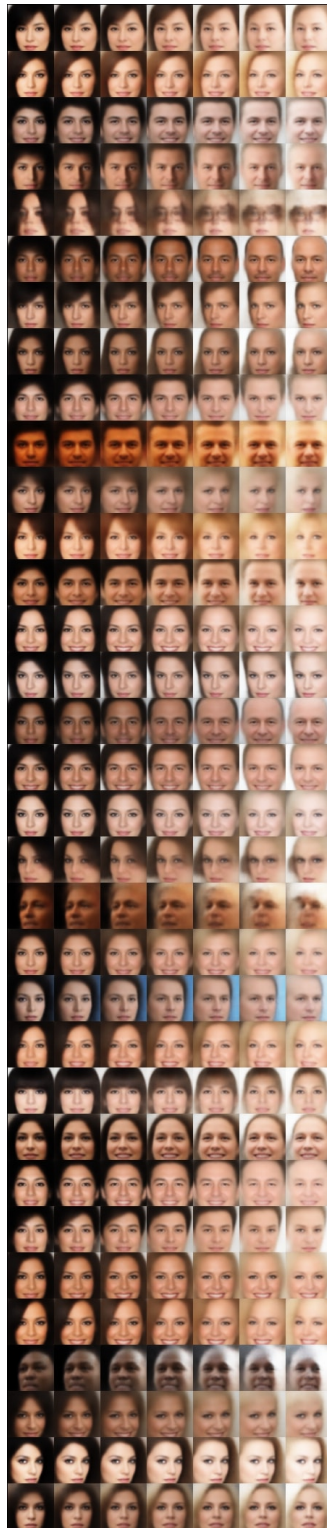
Gender



# Isolating Sources of Disentanglement in Variational Autoencoders



Skin color



Brightness



Bangs (side)

# Isolating Sources of Disentanglement in Variational Autoencoders



Hue



Face width



Eye shadow